International Journal of Thermal Sciences 85 (2014) 73–92

Contents lists available at ScienceDirect

International Journal of Thermal Sciences

journal homepage: www.elsevier.com/locate/ijts

Review

Twenty first century cooling solution: Microchannel heat sinks

Sambhaji T. Kadam, Ritunesh Kumar*

Mechanical Engineering Department, Indian Institute of Technology Indore, MP 453446, India

ARTICLE INFO

Article history:
Received 8 February 2014
Received in revised form
11 May 2014
Accepted 11 June 2014
Available online 12 July 2014

Keywords:
Microchannels
Flow visualization
Pressure drop
Heat transfer coefficient
Instability

ABSTRACT

Due to rapid evolution in a wide range of technologies in twentieth century, heat dissipation requirement has increased very rapidly especially from compact systems. There is an urgent need for high-performance heat sinks to ensure the integrity and long life of these petite systems. Use of forced convection cooling has been limited by the requirement of the excessively high flow velocity and associated noise and vibration problems. Microchannel heat sink seems to be most reliable cooling technology due to its superior command over heat carrying capability. Understanding the flow boiling phenomena in microchannel heat sink experimentally and analytically has been topic of intense research in twenty first century. In this review paper, the experimental studies on flow visualization, pressure drop and heat transfer characteristics of microchannels presented by different researchers are summarized. Some different flow patterns observed in microchannel geometry such as bubble nucleation in thin film, periodic variation of flow pattern, flow circulation, bubble suppression and cross-channel flow are explained briefly. The influence of vapour quality, heat flux, mass flux and channel geometry on pressure drop and heat transfer characteristics of microchannel are reported. Different correlations reported for single and two phase heat transfer characteristics are compared. The comparative analysis showed that available single phase and two phase correlations are inconsistence and large variation is observed among these correlations for same channel geometry, fluid and operating condition. Different instabilities associated with microchannels are also briefly presented.

1. Introduction

With advancement in almost all technology sectors, the world is moving towards miniaturization. Hence, it becomes necessary to remove high heat flux from highly compact systems such as high-performance computer chips, laser diodes and nuclear fusion and fission reactors for ensuring their consistent performance with long life. Heat generated per unit area has measured up to 10^4 W/cm^2 (nuclear reactor). Microchannels and minichannels are naturally well suited for this task, as they provide large heat transfer surface area per unit fluid flow volume. Hence, facilitating very high heat transfer rate. Use of microchannels can be explored in various applications i.e. turbine blades, rocket engine, hybrid vehicle, hydrogen storage, refrigeration cooling, thermal control in microgravity and capillary pump loops [1]. Heat flux removal requirement varies significantly based on the type of application. For densely packed integrated circuit (ICs) [2,3] and laser mirror [4] the maximum power flux reported is 10^2 W/cm^2, aviation and VLSI industry need up to 10^3 W/cm^2 [5] and fusion reactor and defence application contain components that require heat flux removal rate of the order of 10^4 W/cm^2 [6,7]. Kandlikar [8] reported that the use of enhanced microchannel geometry may provide heat dissipation rate up to 10^3 W/cm^2. Heat dissipation requirement will continue to rise with more advancement in technologies and further reduction in the size of these applications. Considering above facts, it can be concluded that microchannel heat sinks seem to be the plausible solution of twenty first century cooling problems.

In order to overcome the problem of high heat flux removal from small area, first time Tuckerman and Pease [9] had developed microchannel heat sink made up of silicon to remove heat flux of 790 W/cm^2 with water as working fluid. They found that the performance of VLSI circuit was accelerated with such type of microchannel heat sink. Keyes [10] carried out theoretical analysis of finned microchannel heat sink with conventional heat exchanger theory and concluded that the size of fin and channel dimensions could be optimized to provide maximum cooling under wide range of application. Thermal performance tests were conducted on silicon and indium phosphate microchannel heat sinks by Phillips [4]. He found that the thermal performance of microchannel heat sink was approximately two times better than conventional channel

* Corresponding author. Tel.: +91 7324 240734; fax: +91 7324 240761.
E-mail address: ritunesh@iiti.ac.in (R. Kumar).

http://dx.doi.org/10.1016/j.ijthermalsci.2014.06.013
1290-0729/

heat sink. Missaggia et al. [11] developed a microchannel heat sink (40 channels of dimension (W, H) (100, 400) μm made through etching on silicon wafer) for cooling of two dimensional high power density diode laser arrays, the use of microchannel heat sink provided significant increase in optical power output.

Classification of the microchannel is controversial issues. Some authors have classified based on channel dimension, whereas others believe that it should be based on flow stability. Following is the summery of criteria reported in literature to distinguish between microchannel and macrochannel. Kandlikar and Grande [12,13] had proposed the range as $10 \leq D \leq 200$ μm and Mehendale et al. [14] had suggested the range as $1 \leq D \leq 100$ μm for indentifying microchannel, where D is the diameter of tube or smallest dimension for other cross-sections. Cornwell and Kew [15] and Kew and Cornwell [16] had defined the confinement number (Co) in order to distinguish between macro to microscale flow boiling as given by Equation (1);

$$Co = \left[\frac{\sigma}{g(\rho_l - \rho_v)D_h^2}\right]^{1/2} \quad (1)$$

As per their proposed criteria, channels with $Co \geq 0.5$ can be classified as microchannels, as influence of the gravity was surpassed by the surface tension above this level.

Manufacturing of the microchannel of required shape and size on required material is another major issue. Researchers have used different manufacturing techniques for the fabrication of microchannel. Table 1 summarizes few of the typical manufacturing techniques and the type of microchannel produced. Kandlikar and Grande [12,13] had reported that the technology to fabricate microchannels had quickly evolved from the miniaturization of traditional machining techniques (milling and sawing) to the adoption of modern techniques (anisotropic wet chemical etching, dry plasma etching and surface micromachining, LASER cutting) used in the semiconductor manufacturing industry. These techniques have changed the scenario of microchannel heat sink field, lot of companies i.e. IBM Zurich Research laboratory, AAVID THERMALLOY, Furukawa electric Co., Ltd. and Siliton R&D Corporation have come in business related with microchannels.

Table 2, presents the summary of geometric parameter of microchannels, working fluid and operating conditions used by different researchers, Fig. 1 shows typical parallel microchannel heat sink and different cross sections of microchannel used. It can be concluded from Table 2 that majority of studies have been carried out on copper and silicon substrate based test sections. Copper is very popular material in thermal process equipments due its high thermal conductivity and silicon is good semiconductor extensively used in VLSI and electronics industries. From Table 2, it can also be concluded that most of studies have been carried out by using water or refrigerant as working fluid. Water is not an appropriate coolant for electronic devices due to its current carrying capability and corrosive nature, which may be responsible for complete burnout of electronic devices or scale formation hampering heat transfer characteristics. However, common refrigerants used in field of microchannel heat sink are R410A, R134a, FC-72, FC-77, HFE-7000 and HFE-7100. Table 3 compares thermo-physical properties, ODP and GDP values of different refrigerant. Thermophysical properties play an important role in boiling process like high viscosity of liquid phase, stabilizes thin liquid layer in slug flow and annular flow. Hence, ensure smooth boiling process (by slowing down flow instabilities). Similarly, large density of vapour will facilitate boiling process by ensuring more energetic vapour bubbles (vapour bubble will travel along heated wall after departure, discussed in the flow visualization section) are generated in boiling process. High liquid density is not desirable as it tries to suppress growth of bubble. Whereas, low enthalpy of vaporization, activates large number of nucleation site at early stage. Hence, facilitating boiling process and reduces the thermal non equilibrium of liquid and vapour phase. Thus, low enthalpy of vaporization also helps reducing the boiling instabilities associated with microchannel.

In this paper effort has been put to study different flow patterns observed, pressure drop characteristics, heat transfer characteristics and flow instability in microchannels. Dependency of pressure drop and heat transfer characteristics of microchannels on various parameters is described in pressure drop and heat transfer section. Eventually, instabilities associated with microchannels such as flow reversal, pressure fluctuation, wall temperature fluctuation and Ledinegg instability are addressed.

Table 1
Different microchannel fabrication techniques.

Author	Process	Material	Dimensions (W, H) μm
Papautsky et al. [17]	Electroplating	Silicon and glass	Rectangular, $W = 300-1500$, $H = 50-100$
Lee et al. [18]	Micro-milling	Copper	Rectangular, $W = 194-534$, $H = 5^*W$
Wu and Cheng [19]	Photolithography method	Silicon	Trapezoidal, $W_1 = 251$, $W_2 = 155.7$, $H = 56.5$
Mei et al. [20]	Micro-moulding	Copper and aluminium	Rectangular, $W = 137-174$, $H = 400$
Wu et al. [21]	Deep reactive chemical etching	Silicon	Rectangular, $W = 483.4$, $H = 50$
Chen and Garimella [22]	Saw- Cutting	Silicon	Rectangular, $W = 100$, $H = 389$
Lee et al. [23]	Dry Etching	Silicon	Rectangular, $W = 100$, $H = 100$
Hwang et al. [24]	Laser	Mythacrylate	Circular, $D_h = 8-20$

2. Flow visualization

The study of different flow regimes that exist in microchannels is important because the pressure drop and heat transfer characteristics can not be predicted accurately in absence of comprehensive information about different types flow regime. It is very difficult to predict the sequence of flow patterns in microchannels unlike conventional channels without high speed photography. In conventional channels as explained by Thome [52], the sequence of flow pattern is bubbly, slug, churn, wispy-annular and annular flow in vertical flow, whereas for the horizontal flow bubbly, slug, plug, annular, stratified, annular with mist and wave flow exists, as shown Fig. 2(a) and (b), respectively. In case of microchannels flow patterns are quite different than conventional channels. Hence, two phase flow pattern maps and flow boiling heat transfer methods developed for macrochannels fail to predict behaviour of microchannels through simple extrapolation. Pfahler et al. [53] carried out experiments on three different microchannels (W, H) (100, 8) (100, 17) and (53, 135). They found that the largest cross section channel roughly followed Navier–Stokes equation. However, as the channel size reduced, they observed significant deviation from Navier–Stokes prediction.

In the last two decades various researchers have carried out flow visualization study on a single microchannel, multiple microchannels and microtubes.

Sobierska et al. [37] performed experiments using water in a single rectangular microchannel (W, H) (2000, 860) and observed bubbly, slug and annular flow. Lee and Mudawar [5] visualized the

Table 2
Summary of microchannel geometry and operating parameters.

Sr no	Author	Fluid	Microchannel geometry (W, H, D) (μm)	Material	Operating condition
1	Tuckerman and Pease [9]	Water	Rectangular, W = 56, 50, 55, H = 320, 287, 302	Silicon	P_{in} = 1–2 bar, q = 1810–7900 kW/m^2, $\dot{V}$ = 4.7 × 10^{-6}– 8.6 × 10^{-6} m^3/s
2	Peng and Wang [25]	Dionised water	Rectangular, W = 600, H = 700	Stainless steel	T_{in} = 30–60 °C, G = 1480–3947 kg/m^2 s
3	Qu and Mudawar [26]	Water	Rectangular, W = 231, H = 713, N = 21	Copper	G = 135–402 kg/m^2 s, T_{in} = 30, 60 °C, P_{out} = 1.17 bar
4	Qu and Mudawar [27]	Deionised water	Rectangular, W = 215, H = 821, L = 44.8 mm	Copper	G = 86–368 kg/m^2 s, T_{in} = 30, 60 °C, P_{out} = 1.13 bar
5	Steinke and Kandlikar [28]	Water	Rectangular, W = 214, H = 200, L = 57.15 mm	Copper	G = 157–1782 kg/m^2 s, q = 5–930 kW/m^2, T_{in} = 22 °C, P_{out} = 1.13 bar, x = 0–1
5	Coleman and Krause [29]	R134a	D_h = 830, L = 5 mm, N = 18 ports		G = 185–785 kg/m^2 s
6	Lee et al. [30]	Deionised Water	Trapezoidal, W_1 = 102.8, W_2 = 59.18, H = 30.1, N = 1	Silicon	q = 1.47–449 kW/m^2, G = 170–477 kg/m^2 s
7	Li et al. [31]	Deionised water	Trapezoidal, W_1 = 100, W_2 = 41, H = 41, N = 2	Silicon	q = 12.4–303 kW/m^2 G = 105–555 kg/m^2 s
8	Lee and Mudawar [32]	R134a	Rectangular, W = 231, H = 713 μm	Copper	P = 1.44–6.6 bar, x_{in} = 0.001–0.25, x_{out} = 0.49–superheated, q = 316–938 kW/m^2, G = 127–654 kg/m^2 s
9	Kosar et al. [33]	Water	Rectangular, W = 200, H = 264, L = 10 mm, N = 5	Silicon	q = 280–4450 kW/m^2, G = 41–302 kg/m^2 s
10	Ling et al. [34]	Distilled water	D = 13, 20, L = 40–100 mm	Silex glass	At room temperature
11	Chen and Garimella [35]	FC-77	Rectangular, W = 389, H = 389, N = 24	Silicon	T_{in} = 71 °C, P_{exit} = 1 atm., q = 94–617 kW/m^2, $\dot{m}$ = 35, 47, 60 ml/min
12	Yun et al. [36]	R410a	Rectangular, D_h = 1360 (N = 8), 1440 (N = 7)		T_{sat} = 0, 5, 10 °C, q = 10–20 kW/m^2, G = 200–400 kg/m^2 s
13	Sobierska et al. [37]	Water	Rectangular, W = 860, H = 2000, L = 330 mm, N = 1	Copper	T_{sub} = 2–20 K, T_{in} = 36.4–36.5, P_{out} = 1 atm., q = 100 kW/m^2, G = 50–1000 kg/m^2 s
14	Huh et al. [38]	Deionised water	Rectangular, W = 100, H = 107	Silicon	P_{out} = 1 atm., q = 200–530 kW/m^2, G = 170, 360 kg/m^2 s
14	Qi et al. [39]	Liquid nitrogen	Circular tube, D = 531, 834, 1042, 1931, N = 1	Stainless steel	Re = 10,000–90,000, system pressure = 1–9 bar
15	Lee and Mudawar [5]	HFE-7100	Rectangular, W = 123.4–259, H = 304.9–1041.3, L = 10 mm, N = 24, 11	Copper	T_{in} = −30 °C, P_{out} = 1.138 bar, q = 0–7500 kW/m^2, G = 670–6730 kg/m^3 s
16	Wang et al. [40]	Water	Trapezoidal, W_1 = 427, W_2 = 208, H = 146, N = 8	Silicon	T_{in} = 35 °C, q = 184.2–485.5 kW/m^2
17	Agostini et al. [41]	R134a	Circular, D = 509, 790	Glass	T_{in} = 30 °C, q = 6.5–31.8 kW/m^2, G = 200–1500 kg/m^2 s, x = 0.02–0.19
18	Singh et al. [42]	Water	D_h = 142 constant, L = 20 mm, β = 1.24, 1.43, 1.56, 1.73, 2.56, 3.6, 3.75, N = 1	Silicon	q = 290–366 kW/m^2, G = 82.4–126.2 kg/m^2 s
19	Ergu et al. [43]	Distilled Water, Potassium ferricyanite	Rectangular, W = 3700, H = 107.9, L = 35 mm, N = 1	Acrylic	T_{in} = 25 °C, for pressure drop: Re = 100–845, for mass transfer: Re = 18–550
20	Schilder et al. [44]	Ethanol and water	Circular tube, D_h = 600, L = 110 mm	Glass	T_{in} = 23 °C, G = 158–317 kg/m^2 s, q = 50–97 kW/m^2, Re = 25–202
21	Krishnamurthy and pales [45]	HFE-7000	Rectangular, W = 200, H = 243, L = 10 mm, N = 5, pin: D = 100 μm dia, N = 24, pitch ratio = 4	Silicon	q = 100–1100 kW/m^2, G = 350–827 kg/m^2 s
22	Balasubramanian et al. [46]	Deionised water	Rectangular, W = 300, aspect ratio = 4, N = 40	Copper	T_{in} = 90 °C, q = 1400 kW/m^2, G = 100–133 kg/m^2 s
23	Megahed [47]	FC-72	Rectangular, W = 225, H = 276, L = 16 mm, N = 45, Three cross linked channel 500 μm wide,	Silicon	q = 7.2–104.2 kW/m^2, G = 99–290 kg/m^2 s, X_{out} = 0.01–0.71
24	Barlak et al. [48]	Distilled Water	Circular, D_h = 200–589, L/D = 16–265	Stainless	T_{in} = 25 °C, Re = 100–1000
25	Edel and Mukherjee [49]	Water	Rectangular, W = 201, H = 266, L = 25 mm, N = 1	Brass	T_{in} = 64, 80, 98 °C, $\dot{m}$ = 0.41–0.82 ml/min
26	Lu and Pan [50]	Water	Rectangular varying cross section, inlet: W = 100, H = 76, outlet: W = 560, H = 76, N = 10	Silicon	G = 99–293 kg/m^2 s
27	Lee et al. [23]	Water	Rectangular, W = 50, 100, H = 46, 48, 100, L = 64 mm, N = 1	Silicon	P_{in} = 1–10.15 bar, T_{in} = 24 °C, G = 138.9 kg/m^2 s
28	Park et al. [51]	FC-72	Rectangular, D_h = 67 (N = 190), D_h = 278 (N = 95).	Stainless steel	Case I: D_h = 67, q = 0.6–3.6 kW/m^2, G = 188–742 kg/m^2 s Case II: D_h = 278, q = 6–45.1 kW/m^2, G = 449–1538 kg/m^2 s

nucleate flow boiling at inlet, middle and outlet section of microchannel and related the flow patterns with boiling curve. Megahed and Hassan [54] carried out experiments on 45 rectangular microchannels (W, H) (225, 276) with FC-72 as working fluid over wide range of the heat flux (q = 60.4–130.6 kW/m^2) and mass flux (G = 341–531 kg/m^2 s). They concluded that two phase flow in microchannel can be divided into three main flow regimes; bubble, slug and annular flow. Zhang and Fu [55] performed experiments on vertically upward microtubes of 531 and 1042 μm inner diameter using liquid nitrogen as working fluid. They reported bubbly flow, slug flow, churn flow and annular flow as the main flow patterns. They also observed confined bubble flow (Fig. 3(a)), mist flow, bubble condensation (Fig. 3(b)) and flow oscillation in their study. Two types of flow pattern were reported by Kawahara et al. [56]; (a) quasi-homogeneous (Fig. 3(c)): shorter gas plugs at high liquid flux (b) quasi-separated (Fig. 3(d)): longer gas bubble

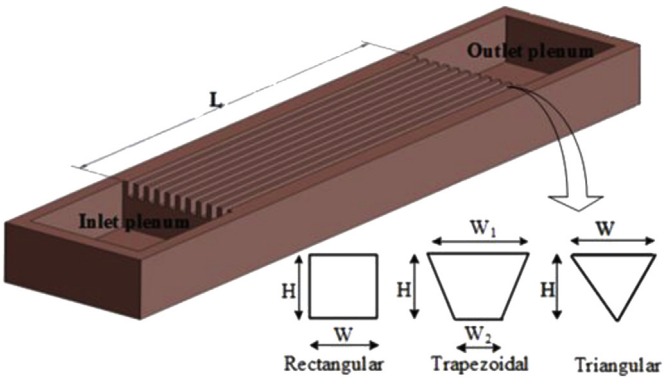

Fig. 1. Parallel microchannel heat sink.

surrounded by smooth and wavy liquid film at high gas flux. Experiments were performed by mixing Nitrogen gas with distilled water and aqueous solution of ethanol on circular tube of diameter 250 μm. Choi and Kim [57] carried out water and Nitrogen-gas two-phase flow experiments over range of superficial velocity of liquid (0.06–1.0 m/s) and gas (0.06–72 m/s) on five different types of rectangular microchannels (D_h = 141, 143, 304, 322 and 490). They reported the bubbly flow, slug bubble flow, elongated bubble flow (Fig. 3(e)), transition flow and liquid ring flow (Fig. 3(f)) in their flow visualization study. The elongated bubble flow and the liquid ring flow are repeated periodically in transition flow. Choi et al. [58] observed bubbly flow, transition flow and liquid ring flow on rectangular microchannels of varying aspect ratio (α = 0.16, 0.47, 0.67, 0.92). They found that two phase flow became homogeneous with decrease in aspect ratio, which they attributed to decreased liquid thickness at low aspect ratio. Cornwell and Kew [15] conducted experiments with R-113 flowing inside rectangular microchannels of size (W, H) (1200, 900). They reported three flow patterns isolated bubble (≈bubbly flow), confined bubble and annular flow in their experimental study.

Kasza et al. [59] performed experiments on small channel of D_h = 3.53 mm. They observed small size nucleating bubble under the thin liquid film that formed between channel wall and vapour core during the slug flow as shown in Fig. 3(g). Similar situation is even possible in case of microchannels but observing such small vapour bubble underneath liquid layer is quite difficult in case of microchannels, dominating surface tension effect worsens the situation.

Chung and Kawaji [60] performed experiments on four microtubes (D = 50, 100, 250, 530), using mixture of water and nitrogen gas as working fluid. They observed the bubbly, slug, swirling pattern in churn flow (Fig. 3(h)), serpentine-like gas core in churn flow (Fig. 3(i)), liquid bridge in slug-annular flow (Fig. 3(j)) and fully developed annular flow for tubes with 250 and 500 μm diameter. Bubbly, churn, slug-annular flows were absent for 50 and 100 μm tubes. The serpentine-like gas flow was having meandering motion. This was attributed to the strong effect of surface tension and liquid viscosity in 50 and 100 μm tubes, which prohibited the turbulence.

Lee and Mudawar [61] carried out experiments to study the two phase flow patterns in test specimen with 53 rectangular microchannels (W, H) (231, 713) for R134a at different heat flux and inlet quality. They observed that bubbly flow regime and nucleate boiling occurred only at low qualities (x_e < 0.05) corresponding to low heat fluxes. Whereas, annular film evaporation flow dominated at high heat fluxes producing medium quality (0.05 < x_e < 0.55) or high quality (0.55 < x_e < 1.0).

Chen and Garimella [35] carried out flow visualization study of test specimen with 24 square microchannels of 389 μm side dimension. They performed experiments under wide range of heat and mass flux. They observed that at low heat fluxes, bubbly flow was dominant, with the bubbles coalescing to form vapour slugs with increase in heat flux. At high heat fluxes, the flow regimes after slug flow in the downstream portion of the microchannels had characteristic of alternating wispy-annular flow and churn flow (Fig. 4), while flow reversal was observed in the upstream region near the microchannel inlet. They attributed the alternating flow patterns to the flow reversal towards upstream and found that flow reversal continued as heat flux was increased and it lasted until the complete dryout of the channel was reached.

Wang et al. [40] carried out flow visualization study in parallel microchannels with three different types of inlet/outlet configurations. Type-A had inlet and outlet port perpendicular to the microchannels. In Type-B, flow entering to and exiting from microchannels freely without restriction. Type-C had inlet restrictions of triangular shape and flow entering with restriction and exiting without restriction in microchannels. They observed that the flow pattern changed with operating condition as well as inlet/outlet configuration. With B type configuration, steady bubbly/slug flow regimes were observed for vapour quality x_e < 0.044, in the range from 0.044 < x_e < 0.103, bubbly/annular alternating flow regimes were observed and for the value of vapour quality x_e > 0.103, annular/mist alternating flow were observed. With C type configuration, bubbly, elongated bubble and annular flow were the main flow regimes observed.

Kashid et al. [62] reported circulation of the liquid behind bubble as shown in Fig. 3(k) within the liquid slug. Which they attributed to the formation of vacuum generated behind the rapidly moving vapour bubble that caused the recirculation of liquid at nose of the upcoming bubble. They further concluded that the recirculation may cause bubble distortion at tail of leading bubble or at nose of upcoming bubble. Agostini et al. [41] observed similar distortion at the tail of elongated bubbles in their study.

Schilder et al. [44] observed in their flow visualization study that the bubble growth took place in both upstream and downstream directions leaving behind a thin evaporating wavy liquid

Table 3
Thermo-physical properties, global warming potential and ozone depletion potential index of different refrigerants.

Refrigerant	Dynamic viscosity (10^{-4} kg/m s)	Liquid density (kg/m^3)	Vapour density (kg/m^3)	Thermal conductivity (W/m K)	Enthalpy of evaporation (kJ/kg)	Surface tension (N/m)	ODP	GWP
R-134a	1.95	1206	32.35	0.081	177.78	0.0080	0	1300
R410a	1.84	1189	29.94	0.076	185	0.0091	0	1890
FC-72	6.40	1680	13.23[a]	0.057	88	0.0105	0	9000
FC-77	6.14	1664	16.63[a]	0.059	89	0.0130	0	9000
HFE-7000	6.00	1400	5.71	0.075	142	0.0124	0	400
HFE-7100	6.10	1520	9.87[#]	0.062	125	0.0136	0	320
R-600a	1.50	549	9.12	0.088	229	0.0101	0	4
R290	0.97	492	21.18	0.094	335	0.0070	0	3

Courtesy: properties collected from various websites and product data sheets.
[a] T_s = 56.6 °C, # P_{sat} = 1 bar, ODP = Ozone Depletion Potential.

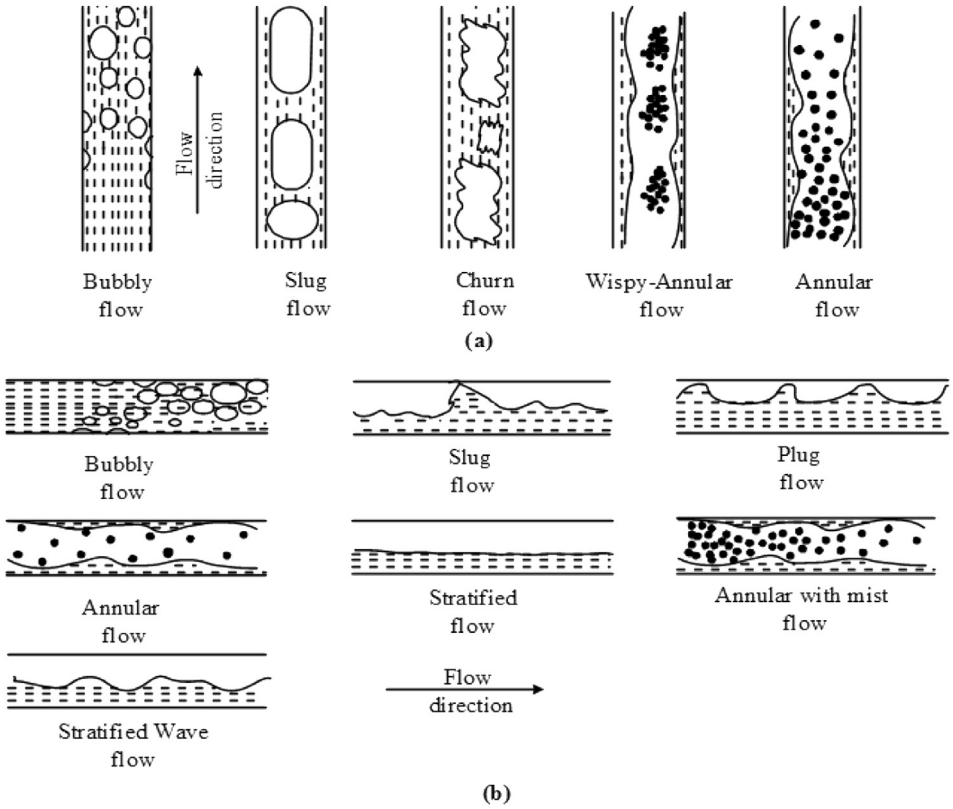

Fig. 2. Flow patterns in conventional channel (a) vertical channel, (b) horizontal channel.

film on the tube. They attributed the shear between vapour and liquid phase during slug flow for the formation of wavy pattern on the film surface. Lee et al. [23] also carried out similar flow visualization study for microchannel with single artificial cavity. An explosive bubble growth was observed at cavity due to high degree of superheat at artificial nucleation site. Krishnamurthy and Peles [45] observed the flow for rectangular microchannels ($D_h = 222$ μm) containing a single row of 24 pin fin of 100 μm in diameter. Flow visualization revealed the existence of isolated bubbles, bubbles interacting (Fig. 3(l)), multiple flow and annular flow.

Barber et al. [63] had observed the variation in interfacial velocities of growing vapour slug over time along with bubble nucleation and growth in a single microchannel ($D_h = 727$) using refrigerant FC-72. The downstream end of the bubble was called as nose and upstream end was named as bubble tail. The tail and the nose moved with same velocity until bubble was not confined. After confinement, tail velocity was reduced due to inertia of incoming fluid suppressing the bubble tail. Whereas, the bubble nose velocity increased as negligible resistance of fluid was present in downstream direction.

Megahed [47] carried out flow visualization study on 45 straight microchannels ($D_h = 727$) connected through three cross-links of width 500 μm. They carried out experiments under heat flux range (37–69.6 kW/m^2), mass flux range (109–195 kg/m^2 s) and vapour quality range (0.2–0.4). They observed only slug flow under entire range of experimentation. They did not observe transition from slug flow to annular flow, which they attributed to transverse flow within the cross link.

Edel and Mukherjee [49] observed that elongation of the vapour bubble after confinement Fig. 5(a)–(b) resulted into suppression of preceding vapour bubble. As vapour bubble started expanding after confinement, pressure spike was generated in upstream direction. This pressure suppressed preceding bubble, hence the size of preceding bubble was reduced as shown in Fig. 5(c). This smaller size bubble again started growing, when larger bubble pushed enough liquid out of the channel for decreasing built up pressure as shown in Fig. 5(d). The small vapour bubble growth continued until it pushed larger bubble out of the channel, as shown in Fig. 5(e). Entire process repeated itself in the same sequence after some time interval.

David et al. [64] performed experiments with single copper microchannel (W, H) (124, 94) using mixture of air and water as working fluid. One side wall of the microchannel was made up off the hydrophobic Teflon membrane of 65 μm thicknesses and 220 nm pore diameter in order to study the effect of venting process. This wall acted as venting wall, which helped in removing the air only through it, thus avoiding instability due to vapour locking. Air was injected from opposite site of hydrophobic thin membrane. They also observed that with increase in inlet air flow, flow patterns followed sequence of bubble, wavy, wavy-stratified, stratified, slug annular, annular at constant water flow rate. At higher water flow rates, jetting type breakup was observed and no air venting could take place as annular flow followed by jetting type breakup. Table 4 presents main summary of few important flow visualization studies.

Use of flow map for predicting two phase pattern is extremely popular and well established for conventional size channels [65–69]. Flow map is basically two–dimensional graph with transition criteria for separating various flow regimes of two phase flow. As the state is transformed towards boundary (separating two regimes), it become unstable and further transition beyond boundary converts flow patterns. Few authors have tried to develop flow map for microchannel. Perhaps, Triplett et al. [70] were the first to develop flow map for microchannel. They identified the transition boundaries between different flow patterns using gas

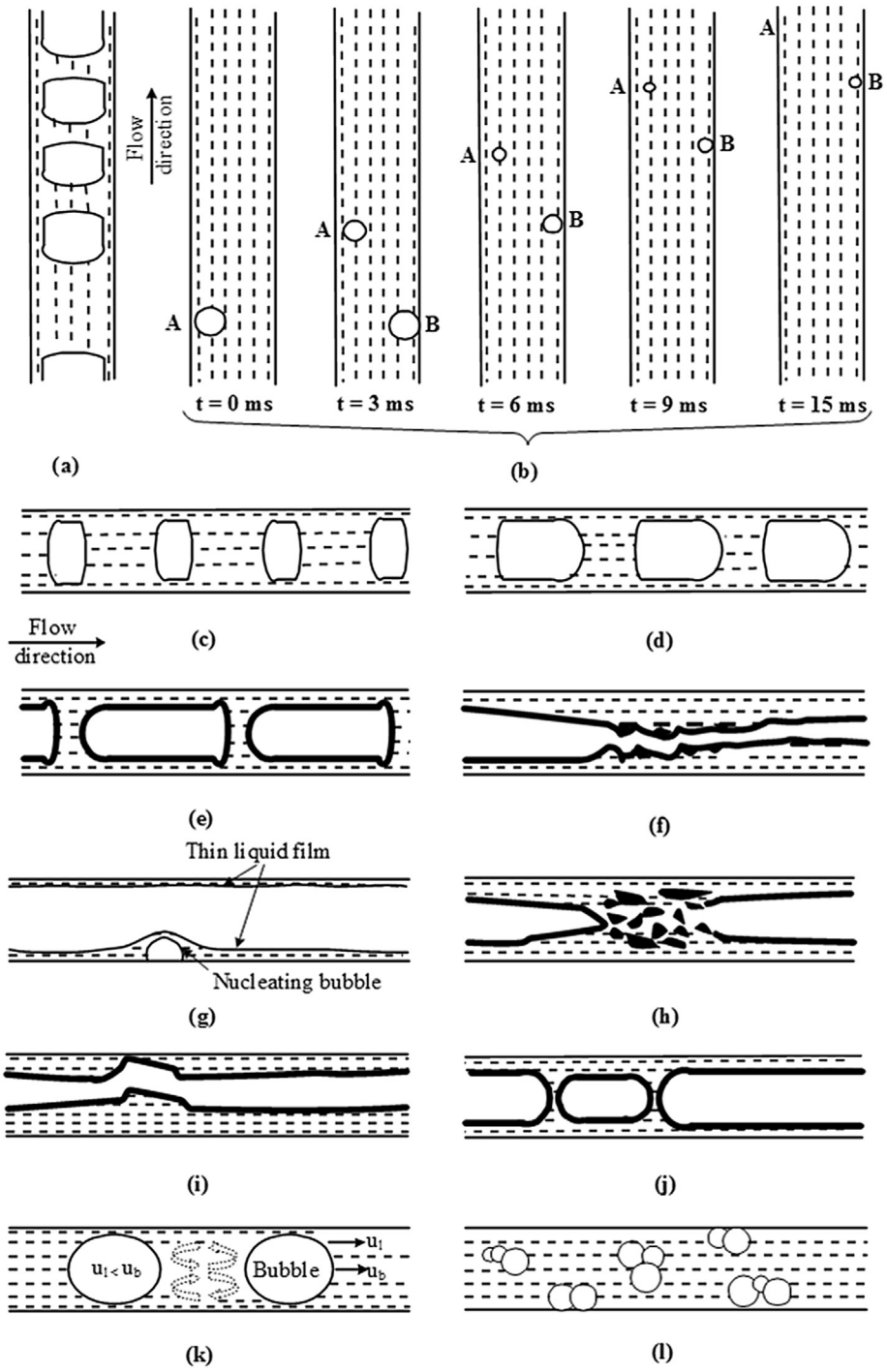

Fig. 3. Various types of flow patterns in microchannel (a) confined bubble flow [55], (b) bubble condensation [55], (c) quasi-homogeneous flow [56], (d) quasi-separated flow [56], (e) elongated bubble flow [57], (f) liquid ring flow [57], (g) bubble nucleation in the liquid film [59], (h) swirling pattern in churn flow [60], (i) serpentine-like gas core in churn flow [60], (j) liquid bridge in slug-annular flow [60], (k) circulation in microchannel [62], (l) bubble interacting [45].

liquid superficial velocities as coordinates. Harirchian and Garimella [71] developed comprehensive flow regime map for FC−77 using non dimensional form of heat flux ($Bl{\cdot}Re$) as abscissa and convective confinement number ($Bo^{0.5}Re$) as ordinate on flow map. They also suggested new transition criteria ($Bo^{0.5}Re < 160$) for physical confinement in microchannel. Sur and Liu [72] developed flow map for adiabatic air water two phase flow using modified Weber number ($We_G\,(D/\lambda)^2$, We_L) as X and Y coordinates. They also observed that boundary of the annular flow regimes shifted to higher gas superficial velocity as the channel dimension is reduced from 324 μm to 100 μm.

From the reviewed literature related to flow regime map, it has been observed that exact location of the transition boundaries on flow map varies dramatically even for microchannels of same geometry under same flow conditions. More efforts are needed for developing comprehensive flow map for microchannels.

Authors have also studied complete bubble dynamics in microchannel since its inception through flow visualization. Bubble

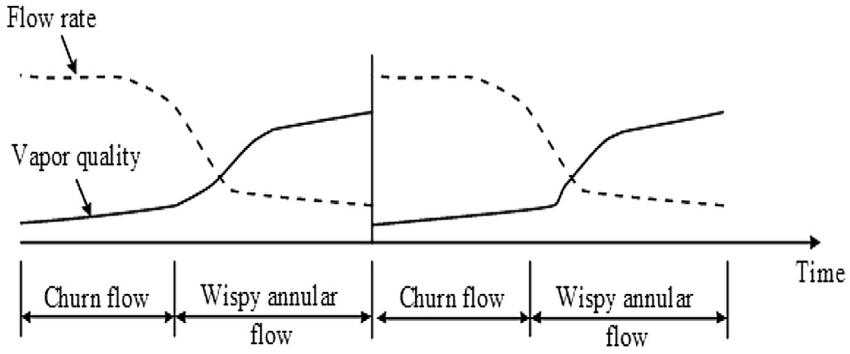

Fig. 4. Periodic variation of flow patterns with time (Chen and Garimella [35]).

dynamics (bubble nucleation, growth, departure and its motion along the flow) plays an important role in heat transfer and pressure drop characteristics as well as various flow instabilities during two phase flow of microchannels. First step in the bubble dynamics is the inception of the bubbles at active nucleation site. Basically, nucleation site is small cavity, where the phase change process starts. Bubble grows for certain duration at nucleation site then it departs from it. Bubble departure diameter from nucleation site governs subsequent bubble dynamics. If departure diameter is around equivalent to channel dimension (in case of high heat flux or very small sized microchannel) then confinement may occurs at nucleation site itself [30,31]. Bubble basically do not detach in such case before start of confinement process. However, if bubble departure diameter is small in comparison to channels dimension then bubble starts travelling along the flow direction [73] at heated surface after departing from nucleation site. Once bubble diameter grows equivalent to channels dimension then confinement process initiates. The bubble growth process rapidly increases after this due to heating from side walls. Once bubble confines complete cross section then starts elongating in flow direction. Elongated bubble finally leaves the microchannel or may lead to flow reversal phenomena (explained in instability section) at high heat flux values. Fig. 6 shows complete bubble dynamics for microchannel.

Hsu [74], first time proposed the phenomena of bubble inception at nucleation site during boiling. As per his theory bubble nucleation is possible only if the minimum surrounding temperature of nucleation site being at least equal to the saturation temperature corresponding to liquid pressure. Bubble growth at nucleation site is divided between two regions; inertia controlled region and diffusion controlled region (Lee et al. [30]; Meder [75]). In the initial stage size of bubble is very small, bubble growth is governed by the reaction force of the surrounding liquid at the bubble interface. This stage is called as inertia controlled region. As the bubble starts growing, thermal diffusion (between vapour liquid interface and surrounding liquid) effect increases. Once it overcomes inertia effect, subsequent bubble growth is governed entirely by thermal diffusion process [76]. Liu et al. [73] observed linear bubble growth at nucleation site from its inception to the departure. Whereas, Lee et al. [30] observed explosive bubble growth also for a few combinations of heat flux and mass flux values. However, they failed to explain reason behind explosive bubble growth. In case of Lee et al. [77] experimental study, bubble even stretched away in flow direction during its growth at nucleation site. Further, they observed that bubble confined entire channel cross-section before departing from the nucleation site.

Kew and Cornwell [16] were first to report the confined bubble growth in case of the small tube. Barber et al. [63] classified the confinement as the partial confinement ($D_{bubble} = \min(W, H)$) and full confinement ($D_{bubble} = \max(W, H)$). They observed that partial confinement produced both radial and elongated growth, whereas

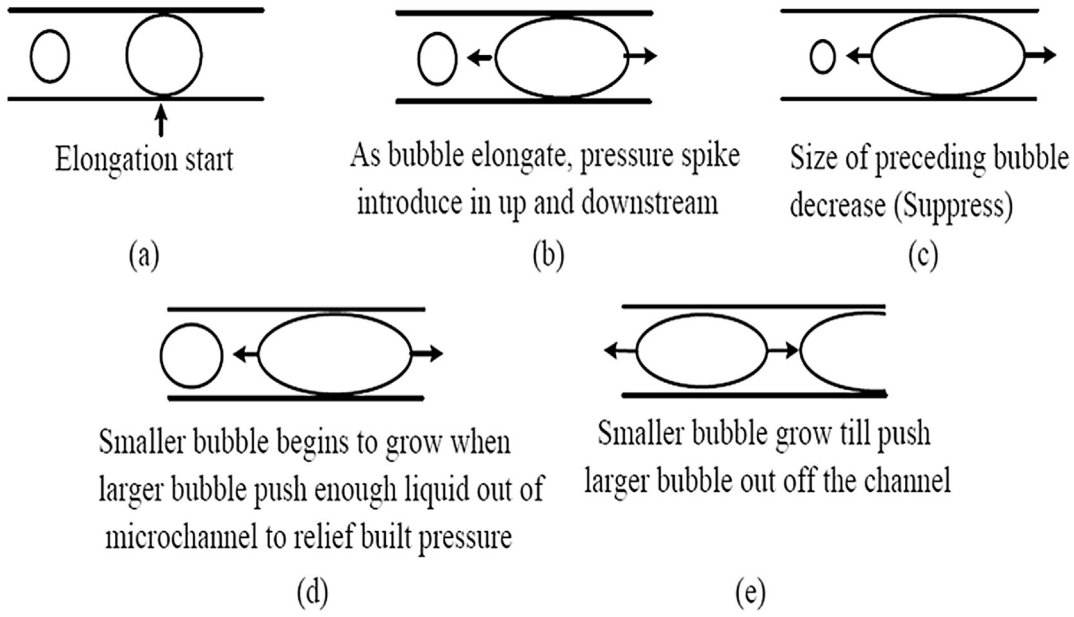

Fig. 5. Sequence of interacting bubble suppression in microchannel (Edel and Mukherjee [49]).

Table 4
Summary of important flow visualization studies.

Author	Remark
Kasza et al. [59]	• Bubble growing pattern inside thin liquid film (below vapour slug) tries to avoid early occurrence of dryout condition
Chung and Kawaji [60]	• They studied effect of microtube diameter on flow pattern
Lee and Mudawar [61]	• Bubbly, slug, alternating wispy-annular flow and churn flow
Schilder et al. [44]	• Temporary dryout can even initiate at low vapour quality due to instable liquid film • Instability issues are more severe in case of low viscous flow
Krishnamurthy and Peles [45]	• Extended surface can help in mitigating early stage flow instability
Megahed [47]	• Flow stability can be improved by mass flux retardation from downward direction
Edel and Mukherjee [49]	• Instability issues easily provoke in case of single microchannel
David et al. [64]	• Bubbly flow was observed towards the end of channel due to air venting by hydrophobic membrane

full confinement was coupled with elongated growth only. Fu et al. [78] carried out bubble growth study before and after bubble departure from nucleation site for minichannel (D = 1.3–1.5 mm) using nitrogen as working fluid. They reported linear and constant bubble growth in both cases. Gedupudi et al. [79] carried out experiments for the studying the growth of confined bubble in rectangular microchannel using water as working fluid. They observed exponential bubble growth after confinement from microchannel wall. Yin et al. [80] concluded that elongation of the bubble after confinement is influenced by effective heat supplied and bubble moving velocity along the flow. Recently, Tuo and Hrnjak [81] carried out complete bubble dynamic study using R134a refrigerant. They observed linear bubble growth before confinement and exponential bubble growth in axial direction after confinement. Exponential bubble growth was accredited to intensive evaporation of thin liquid layer trapped between vapour bubble and microchannel wall.

3. Pressure drop

It is of significant interest to understand the pressure drop characteristics across microchannel, when designing applications based on microchannel. As hydraulic diameter of microchannel is very small, it is expected that single phase pressure drop per unit length associated with microchannel will be much higher than macrochannels under same operating conditions. Boiling in microchannels even promotes the two phase pressure drop associated in comparison to conventional size channels. In spite of being associated with large pressure drop, microchannel heat sinks had attracted lot of attention due to their strong command over heat transfer characteristics. Large pressure drop is responsible for huge power consumption of the pump utilized. Thus, the study of pressure drop in microchannels is equally important similar to other aspects associated. Two phase flow/pressure drop can be modelled using the homogeneous flow model and separated flow model. In homogeneous flow model, two phases (liquid phase and vapour phase) are treated as a single phase. Another fundamental assumption of homogeneous model is that liquid and vapour have equal velocity. The separated flow model considers the phases to be artificially segregated into two streams, one contains only liquid and anther contains only vapour. The fundamental assumption of the separated flow model is that liquid and vapour have constant but not necessarily equal velocities. The pressure drop across the channel is mainly dependent on the fluid properties (density, viscosity and surface tension), mass flux (flow velocity, mass flow rate or Reynolds number), effective heat supplied (wall temperature), vapour quality and channel geometry (aspect ratio, hydraulic ratio and cross section). Various researchers have studied the effect of these parameters on the pressure drop characteristics of microchannels.

Researchers have carried out pressure drop analysis in single phase, two phase with subcooled and saturated inlet condition in microchannels. Very few studies have been carried out in single phase mode. Qu and Mudawar [82] carried out experimental and numerical study to predict the pressure drop for single phase in rectangular microchannel heat sink using water as working fluid. They observed that pressure drop reduced with increase in heat flux at constant Reynolds number. They accredited it to the decrease in viscosity of water at elevated temperature. Ergu et al. [43] carried out experiments in the range of Reynolds number from 100–845 using water as working fluid on rectangular microchannel (W, H) (3700, 107.4). They observed that pressure drop increased linearly with Reynolds number and concluded that single phase pressure drop behaviour of microchannel is very much similar to the macrochannel for laminar flow region. Barlak et al. [48] conducted experiments on microtubes (D = 200, 250, 400, 505 and 589) having L/D ratio in the range of 16–265 using water as cooling fluid. They observed that at low Reynolds number (Re < 2000),

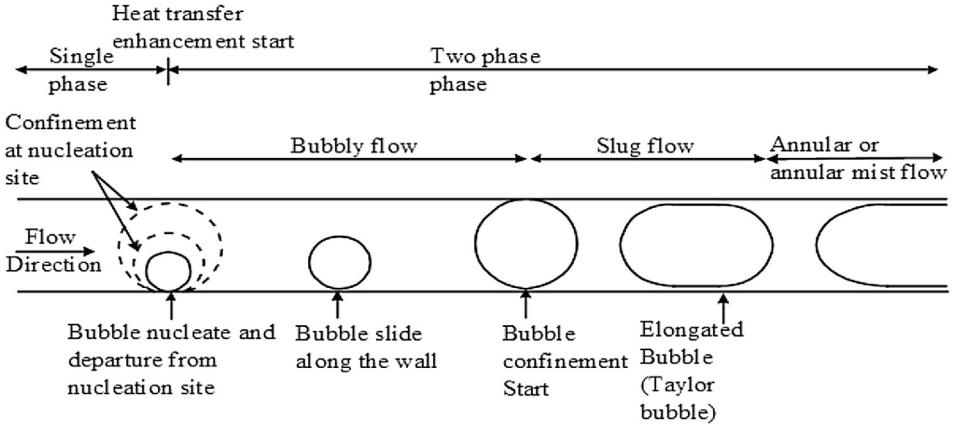

Fig. 6. Complete bubble dynamics in microchannel.

pressure drop was weak function of L/D ratio and linear relationship existed between pressure drop and Reynolds number. Whereas, pressure drop was strongly dependent on L/D ratio at high Reynolds number. Unlike large diameter tubes, smaller diameter tubes faced a noticeable change in pressure drop with L/D ratio beyond $Re > 2000$. Ling et al. [34] carried out pressure drop analysis on circular tubes of 13 and 20 μm diameter and length ranging from 40 to 100 mm under pressure driven force condition. Linear relationship between the flow rate and pressure drop was projected by them. They further concluded that the flow characteristics of the microtubes are basically in agreement with macroscopic liquid flowing lows. Qi et al. [39] carried out pressure drop study on different diameter tubes ($D = 531, 834, 1042$ and 1931) of constant length ($L = 250$ mm) in the range of Reynolds number 10^4–9×10^4. They observed that the total single phase pressure drop increased with increase in mass flux and decrease in tube diameter. It was also observed that friction factor obeyed conventional channel theory for tubes having diameter of 1042 and 1931 μm. However, for the 531 and 834 μm tubes, friction factor value deviated from conventional channel theory. They attributed it to the effect of the surface roughness on friction factor in case of small tubes. Akbari et al. [83] carried out pressure drop analysis on rectangular microchannels of varying aspect ratio in the range of 0.13–0.76. They observed that pressure drop increased with increase in the aspect ratio. However, it increased very rapidly as the width of channel also approached to the limiting criteria of microchannel. They also characterized different type of losses such as contraction and expansion loss, developing region and fully developed region loss and loss due to electro-viscous effect. Peiyi and Little [84] carried out single phase experiments on nitrogen, hydrogen and argon gas with eight different microtubes having diameter ranging from 55.81 to 83.08 μm. They concluded that friction factor is dependent on the channel geometry, roughness and mass flux.

Two phase pressure drop is of significant interest as far as flow boiling in microchannels is concerned. Fig. 7 shows the variation of pressure drop for single phase and two phase with respect to (q''/q''_{sat}) for subcooled boiling and saturated boiling region in horizontal orientation of microchannel, following Lee and Mudawar [85]. In the single phase, pressure drop is primarily governed by the behaviour of liquid viscosity with temperature. For fluid like water pressure drop reduces with increase in wall heat flux at constant mass flux due to decrease in liquid viscosity for single phase region. Pressure drop reduction starts decreasing once onset on nucleate boiling (ONB) condition is approached. ONB is the location, where the first bubble forms. ONB indicates the termination of single phase flow and inception of the subcooled boiling region as shown in Fig. 7. Formation of bubble introduces two phase pressure drop components, frictional and acceleration. The magnitude of these components increases with increase in heat flux due to growth of vapour bubble or due to formation of new bubble at newly activated nucleation sites. They try to pull up pressure drop associated with microchannel unlike viscosity. In subcooled boiling region pressure drop initially reduces after ONB and attains minima. This was attributed to the higher degree of subcooling, which suppressed the bubble growth initially after ONB. On further increase of heat flux beyond minima condition, the vapour bubble pressure drop components become dominating. Therefore, pressure drop starts increasing with increase in heat flux. This trend continued even in saturated boiling region. However, in case of the vertical orientation gravitational pressure drop/gain (upward flow/downward flow) will influence pressure drop characteristics of both single and two phase flow. Gravitational pressure drop/gain is more dominating than frictional pressure drop in case of single phase flow. As flow shifts from single phase to two phase, effect of frictional pressure drop supersede gravitational effect.

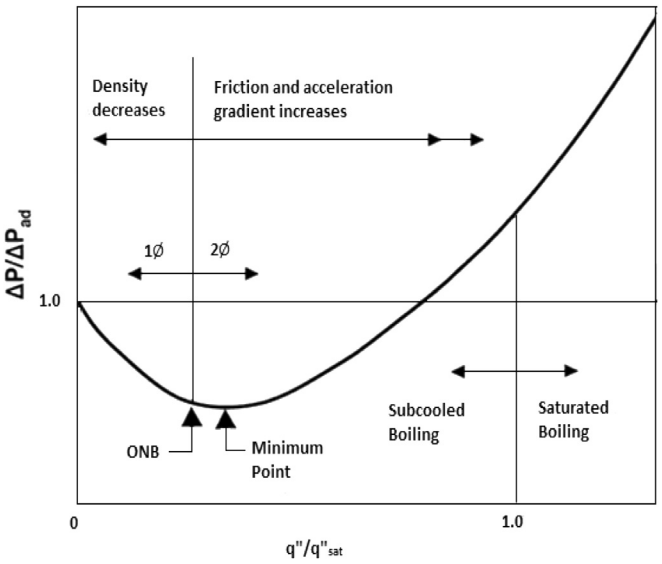

Fig. 7. Normalized plot of pressure drop versus wall heat flux for subcooled boiling (Lee and Mudawar [85]).

Yun et al. [36] carried out two phase experiments on microchannels of hydraulic diameter of 1.44 mm. They found that pressure drop increased with increase in mass flux at constant saturation temperature. At given mass flux, pressure drop decreased with increase in saturation temperature, which they attributed to change in viscosity and density of R410A.

Lee and Mudawar [32] carried out experiments using R134a to study the pressure drop characteristics in microchannels. Based on combined pressure drop data of R134a and water (Qu and Mudawar [86]), they developed two phase pressure drop multiplier empirical relations for separated flow model incorporating liquid viscosity and surface tension effect. These correlations were used to examine the effect of vapour quality, heat flux and mass flux on total pressure drop characteristics of R134a. They found that at constant heat flux total pressure drop decreased with an increase in exit vapour quality, which they attributed to decrease in mass velocity. They also found that for constant mass flux, pressure drop increased up to particular heat flux value beyond which pressure drop became constant or slightly decreased. Up to particular heat flux value, two phase frictional and accelerational losses increases due to conversion of liquid into vapour. After complete conversion into vapour, two phase frictional loss decreases but it is compensated by the increase in single phase vapour pressure loss. However, acceleration loss remains at same value over complete conversion into vapour phase. Thus total pressure drop remained constant or slightly decreased beyond particular heat flux value. Balasubramanian et al. [46] had reported increasing trend of pressure drop for the variation of heat flux at constant mass flux in stepwise expanding microchannels with deionised water. However, they observed that in stepwise expanding microchannels pressure drop decreased with increase in mass flux, which was due to increase in mass flux (inducing reduction in saturation flow length). Reduction in saturation flow length reduces the magnitude of two phase pressure drop per unit length, which is substantially higher than magnitude of single phase pressure drop per unit length. They also observed that pressure drop associated with stepwise expanding microchannel was smaller than straight microchannel, which they attributed to the deceleration of vapour in downstream direction.

Megahed [47] carried out pressure drop analysis of cross linked rectangular microchannels. They observed that two phase pressure drop increased linearly with exit vapour quality at a given mass flux and it increased very rapidly with increase in mass flux at constant vapour quality. They further reported slight increases in slope of pressure drop verses vapour quality line at low mass fluxes (G = 111, 141 kg/m^2 s) and rapid increase in slope at high mass fluxes (G = 191, 245, 290 kg/m^2 s). They accredited it in favour of presence of cross links between microchannels. The presence of cross link also increased associated sudden expansion and contraction pressure losses in addition to increase in pressure loss due to cross flow. Furthermore, they also compared experimental two phase pressure drop data with pressure drop correlations published by Lee and Garimella [87] for straight microchannels. They found that two phase pressure drop in cross link microchannels is almost 1.5 times greater than regular straight microchannels over tested range of mass flux, except at minimum value of mass flux (G = 111 kg/m^2 s). From Balasubramanian et al. [46] and Megahed [47] experimental study, it can be concluded that expanding microchannels have superior pressure drop characteristics than straight and cross link microchannels. Sobierska et al. [37] carried out experiments using water as working fluid on a straight vertical single rectangular microchannel in the range of mass flux from 50 to 1000 kg/m^2 s. They also observed that pressure drop associated with two phase increases with increase in mass flux and exit vapour quality separately. However, pressure drop increased moderately in the range of mass flux (50–300 kg/m^2 s) and rapidly beyond of it. Megahed and Hassan [54] and Park et al. [51] measured experimentally the pressure drop per unit length across rectangular microchannels. In both works, it was observed that pressure drop per unit length increased with increase in mass flux and vapour quality respectively. Megahed and Hassan [54] attributed this behaviour to the impact of void fraction on pressure drop. Park et al. [51] used rectangular microchannels (D_h = 61 and 278 μm) in their experimental study on refrigerant FC 72. They observed that for a microchannel (D_h = 278 μm) at mass flux of G = 112 kg/m^2 s, the pressure drop increased continuously beyond vapour quality of 0.9. This was attributed to the absence of turbulent wave at higher vapour qualities because of very thin liquid film. Eventually, they concluded that existing macroscale pressure drop correlations could not be directly used for microscale (below D_h = 100 μm) due to change in flow patterns below this dimension.

Phan et al. [88] analysed experimentally the effect of surface wettability on two phase pressure drop using four test-sections having single rectangular microchannel (W, H) (5000, 500) and coated with hydrophilic (polydimethylsiloxane (SiO_x), titanium (Ti), diamond like carbon (DLC)) and hydrophobic (polydimethylsiloxane (SiOC)) substances. These surfaces had static contact angle of 29°, 49°, 63° and 103° respectively. They found that at a given mass flux and exit vapour quality, two phase pressure drop increased significantly with increase in static contact angle, which they attributed to the effect of contact angle on surface tension force generated. For unwetted surface (SiOC) having higher contact angle, surface tension force intended to maintain the bubble at the solid wall, which resulted into increase in frictional pressure drop. On the other hand for wetted surface (SiO_x), surface tension helped in proper wetting of the surface. Thus, wetted surfaces were subjected to low two phase pressure drop in comparison to unwetted surface.

Singh et al. [42] investigated the effect of aspect ratio ($\beta = W/H$ = 1.23, 1.44, 1.56, 1.73, 2.56, 3.6 and 3.75) of rectangular microchannel theoretically as well as experimentally. They observed that the pressure drop first reduced with increase in β, attained minima at β = 1.56, then started increasing rapidly with increase in β. The occurrence of minima, they speculated in favour of the opposite nature of frictional and accelerational pressure drop with respect to aspect ratio. With increase in β, acceleration pressure drop decreased and frictional pressure drop increased.

Choi and Kim [57] and Choi et al. [58] carried out experiments using water liquid-nitrogen gas adiabatic two phase flow in microchannel. They concluded that the typical two phase pressure drop characteristics of microchannel can be divided in three regions. Region I: Bubbly flow regime, including bubbly, slug bubble and elongated bubble, Region II: transition flow region, Region III: Liquid ring flow regime. In the Region I, number of bubbles amplified the pressure drop on increase in superficial gas velocity. In the Region II, pressure drop decreased due to collapse of elongated bubble on increase in superficial gas velocity. In the Region III, pressure drop increased very rapidly with increase in superficial gas velocity.

Table 5 summarizes relations proposed by different researches to predict pressure drop across microchannels. Bowers and Mudawar [89] considered the total pressure drop as summation of the single phase, two phase frictional, two phase acceleration and two phase outlet pressure drop components. Qu and Mudawar [86] split the single phase pressure drop into the developing and the fully developed region pressure drop components and also introduced contraction and expansion pressure drop components to calculate exact total pressure drop associated in microchannels. In two phase flow, vapour has higher velocity than the liquid due to its low density in comparison to corresponding liquid phase. In order to accommodate this effect of liquid and vapour, Lee and Mudawar [32] defined two phase frictional pressure drop component in terms of two-phase pressure drop multiplier ($\varnothing$). Two phase pressure drop multiplier was defined in terms of Martinelli parameter (X) and two-phase multiplier parameter (C), which defined the type of the two phase flow (Table 5). Megahed [47] introduced dynamic two phase pressure drop component, which accounted for the enlargement at outlet and bends of microchannels.

4. Heat transfer

Heat transfer coefficient is the most important parameter governing the usefulness of microchannel heat sinks. Heat transfer coefficient for flow boiling in microchannels is impressively high due the combined effect of very small hydraulic diameter and associated latent heat of evaporation. Heat transfer coefficient is primarily influenced by fluid properties (density and viscosity), mass flux, effective heat flux, channel geometry (cross section area and aspect ratio) and vapour quality. Various researchers had carried out experimental studies in single phase as well as two phase heat transfer in microchannels. However, major focus had been given to two phase heat transfer studies.

Peng and Wang [25] studied the effect of force convection on single phase heat transfer characteristics using rectangular microchannels (W, H) (700, 600). They observed that decrease in liquid subcooling and increase in flow velocity induced steep increase in heat transfer coefficient. Wang and Peng [90] also carried out single phase forced convection study using six heat sinks of microchannel dimensions (W, H, N) (800, 700, 4), (600, 700, 4), (400, 700, 4), (400, 700, 6), (200, 700, 4) and (200, 700, 6) using water as working fluid. They observed three different trends for the variation of single phase heat transfer coefficient in above microchannels. In first the trend on (800, 700, 4) heat sink, heat transfer coefficient smoothly increased with wall temperature.

In second trend on (600, 700, 4), (400, 700, 4) and (400, 700, 6) heat sink, steep increase in heat transfer coefficient at low wall temperature was observed. This was followed by moderate increase

Table 5
Summary of pressure drop correlations for microchannel.

Author	Channel geometry and fluid (W, H, D) μm	Operating condition	Correlations
Bowers and Mudawar [89]	Circular, $D = 2540, 510$ R113	$P_{in} = 1.38$ bar, $T_{sub} = 10–32$ °C, $m = 19–95$ ml/min Subcooled boiling and saturated boiling	$\Delta P_T = \Delta P_{sp} + \Delta P_f + \Delta P_a + \Delta P_{out,\ nh}$ $\Delta P_a = \left(\frac{G^2}{\rho_f}\right)\left(\frac{v_{fg}}{v_f}\right)(x_L)$ $\Delta P_{sp} = \frac{2f_{sp}G^2L_{sp}}{\rho_f D}$ $\Delta P_f = \left(\frac{2f_{tp}G^2L_b}{\rho_f D}\right)\left[1+\frac{x_L}{2}\left(\frac{v_{fg}}{v_f}\right)\right]$ $\Delta P_{out} = \left(\frac{2f_{tp}G^2L_o}{\rho_f D_h}\right)\left[1+x_L\left(\frac{v_{fg}}{v_f}\right)\right]$ $f_{sp} = 64/Re$, $f_{tp} = 0.005$
Qu and Mudawar [86]	Rectangular, $W = 231$, $H = 713$ Deionised water	$T_{in} = 30, 60$ °C, $P_{out} = 1.17$ bar, $G = 134.9–400.1$ kg/m^2 s Subcooled boiling and saturated boiling	$\Delta P_T = \Delta P_{c1} + \Delta P_{c2} + \Delta P_{sp,dev} + \Delta P_{sp,fdev} + \Delta P_f + \Delta P_a + \Delta P_{e1} + \Delta P_{e2}$ $\Delta P_{c1} = \frac{v_f}{2}(G_2^2 - G_1^2) + \frac{v_f K_{c1}}{2}G_2^2$ $\Delta P_{c2} = \frac{v_f}{2}(G^2 - G_2^2) + \frac{v_f K_{c2}}{2}G^2$ $\Delta P_{e1} = \frac{v_f + x_e v_{fg}}{2}(G_1^2 - G_2^2) + K_{e1}\frac{(v_f + x_e v_{fg})}{2}G_2^2,\ K_{e1} = \left(1 - \frac{NA}{A_{p2}}\right)^2$ $\Delta P_{e2} = \frac{v_f + x_e v_{fg}}{2}(G_2^2 - G^2) + K_{e2}\frac{(v_f + x_e v_{fg})}{2}G^2,\ K_{e2} = \left(1 - \frac{A_{p2}}{A_{p1}}\right)^2$ $\Delta P_{sp,dev} = \frac{2f_{app}G^2L_{sp,dev}v_f}{D_h}$ $f_{sp,dev}Re_{sp,dev} = 24\,(1 - 1.355\beta + 1.947\beta^2 - 1.701\beta^3 + 0.956\beta^4 - 0.254\beta^5)$ $Re_{sp,d} = \frac{GD_h}{\mu_{sp,dev}};\ \beta = \frac{W}{H}$ $\Delta P_{sp,fd} = \frac{2f_{app}G^2L_{sp,fdev}v_f}{D_h}$ $f_{app} = \frac{1}{Re_{sp,fdev}}\left[3.44(L^+_{sp,fdev})^{-0.5} + \frac{\frac{1.089}{(4L^+_{sp,fdev})} + f_{sp,fdev}Re_{sp,dev} - 3.44(L^+_{sp,fdev})^{-0.5}}{1 + 1.31\times10^{-4}(L^+_{sp,fdev})^{-2}}\right]$ $L^+_{sp,fdev} = \frac{L_{sp,fdev}}{Re_{sp,fdev}D_h};\ Re_{sp,fdev} = \frac{GD_h}{\mu_{sp,fdev}}$ $f_{sp,fdev}Re_{sp,fdev} = 24\,(1 - 1.355\beta + 1.947\beta^2 - 1.701\beta^3 + 0.956\beta^4 - 0.254\beta^5)$ $\Delta P_f = \frac{2f_{tp}G^2L_{tp}v_f}{d_h}\left[1+\frac{x_e}{2}\left(\frac{v_{fg}}{v_f}\right)\right],\ f_{tp} = 0.003$ $\Delta P_a = G^2 v_f x_e$
Lee and Mudawar [32]	Rectangular, $W = 231$, $H = 713$ μm R134a	$P = 1.44–6.6$ bar, $x_{in} = 0.001–0.25$, $x_{out} = 0.49–$superheated, $q = 316–938$ kW/m^2, $G = 127–654$ kg/m^2 s Saturated boiling	$\Delta P_T = \Delta P_c + \Delta P_f + \Delta P_a + \Delta P_{sp,g} - \Delta P_e$ $\Delta P_c = \frac{G^2 v_f}{2}\left[\left(\frac{1}{C_c} - 1\right)^2 + \left(1 - \frac{1}{\sigma_c^2}\right)\right]\left[1 + \frac{v_{fg}x_{e,\ in}}{v_f}\right]$ $\Delta P_e = G^2\sigma_e(1-\sigma_e)v_f\left[1 + \frac{v_{fg}x_{e,out}}{v_f}\right]$ $\Delta P_{sp,g} = \frac{2L_{sp,g}}{D_h}f_{sp,g}G^2v_g$ $f_{sp,g}Re_g = 24(1 - 1.3553\beta + 1.947\beta^2 - 1.701\beta^3 + 0.956\beta^4 - 0.254\beta^5)$ for $Re_g < 2000$ $f_{sp,g} = 0.079Re_g^{-0.25}$ for $2000 < Re_g < 20{,}000$ $f_{sp,g} = 0.046Re_g^{-0.2}$ for $20{,}000 < Re_g$ $\Delta P_a = G^2\left\{\left[\frac{v_g x_{e,out}^2}{\alpha_{out}} + \frac{v_f(1-x_{e,out})^2}{(1-\alpha_{out})}\right] - \left[\frac{v_g x_{e,in}^2}{\alpha_{in}} + \frac{v_f(1-x_{e,in})^2}{(1-\alpha_{in})}\right]\right\}\ \alpha = \left[1 + \left(\frac{1-x}{x}\right)\left(\frac{v_f}{v_g}\right)^{2/3}\right]^{-1}$ $\Delta P_f = \frac{2G^2L_{tp}}{D_h x_e}\int_{x_i}^{x_o} f_f(1-x)v_f\varnothing_f^2 dx,\ \ \varnothing_f^2 = 1 + \frac{C}{X} + \frac{1}{X^2},\ \ X^2 = [(dP/dz)_f/(dP/dz)_g]$ $C_{vv} = 2.15Re_l^{0.047}We_l^{0.6}$ laminar liquid-laminar vapour $C_{vt} = 1.45Re_l^{0.25}We_l^{0.23}$ laminar liquid-turbulent vapour
Megahed [47]	Rectangular, $W = 225$, $H = 276$ FC-72	$q = 7.2–104.2$ kW/m^2, $G = 99–290$ kg/m^2 s, $X_{out} = 0.01–0.71$ subcooled boiling and saturated boiling	$\Delta P_T = \Delta P_{sp} + \Delta P_{tp}$ $\Delta P_{sp} = \frac{\rho_f}{2}\left[\left(\frac{4f_{sp,\ l}L_{sub}}{D_h} + K_c + K_\infty\right)u_{ch}^2 + 2K_{90}u^2\right]$ $L_{sub} = \frac{\dot{m}c_p(T_{sat} - T_{in})}{qA}$ $f_{sp,\ l} = \frac{24}{Re}(1 - 1.3553\beta + 1.9467\beta^2 - 1.7012\beta + 0.9564\beta^4 - 0.2537\beta^5)$ $K_\infty = 0.6796 + 1.2197\beta + 3.3089\beta^2 - 9.5921\beta^3 + 8.9089\beta^4 - 2.9959\beta^5$ K_{90} = bending pressure loss coefficient $\Delta P_{tp} = \Delta P_f + \Delta P_a + \Delta P_{tp,dyn}$ $\Delta P_{tp,dyn} = \frac{G^2 v_f}{2}(1-\sigma_c)^2\left[1 + x_e\left(\frac{v_{fg}}{v_f}\right)\right],\ \sigma_c = \frac{A}{A_p}$ $x_e = \frac{1}{h_{fg}}\left[\frac{Q_{net}}{m} - C_p(T_{sat} - T_{in})\right]$ $Q_{net} = Q_{input} - Q_{loss}$

in heat transfer coefficient at high wall temperature. In third trend on (200, 700, 4) and (200, 700, 4) heat sink, heat transfer coefficient decreased first and then moderately increased as the wall temperature was increased. They further concluded that heat transfer characteristics in laminar and transition region of microchannels are highly complicated compared to conventional channel. This was attributed to the considerable change in thermo-physical properties of the flowing fluid because of large variation in liquid temperature along the length of microchannel. Qu and Mudawar [82] carried out experimental and numerical study of single phase heat transfer using twenty one rectangular microchannels (W, H) (231, 713) heat sink. They compared the result of numerical study with experimental data and suggested that Navier–Stokes and energy equation can successfully predict heat transfer behaviour of the single phase flow. Unlike previous studies, they did not observe the flow transition in the tested range of Reynolds number from 139 to 1672. Qi et al. [39] carried out experiments of the single phase heat transfer analysis on microtube using liquid nitrogen as working fluid. They observed that contrary to water in case of nitrogen heat transfer coefficient and local heat transfer coefficient both decreased in the flow direction with increase in heat flux, which they attributed to the inverse relationship between temperature and thermal conductivity of nitrogen. They concluded that thermal properties of working fluid play an important role on flow and heat transfer characteristics of microchannels. Herwig and Mahulikar [91] had proved importance of change in thermal properties of the working fluid on heat transfer characteristics through their numerical study. Sui et al. [92] carried out experiments using deionized water on three wavy microchannels test pieces (W, H) (205, 404) with different wavy magnitude (0, 138 and 259 μm). They compared the heat transfer performance of the wavy microchannels with straight microchannels and concluded that wavy microchannels had superior heat transfer performance than straight microchannels. They accredited it in favour of secondary flow inside curves of wavy microchannels.

It is widely accepted that the saturation flow boiling in microchannels is governed by nucleate boiling and forced convection boiling (Collier and Thome [93]). The nucleate boiling region is normally associated with the bubbly and slug flow pattern, and the forced convection boiling region is associated with the annular flow pattern. In the nucleate boiling region, the wall temperature is few degree higher than the saturation temperature of the working fluid, which is sufficient for the bubble nucleation and its growth. In this region the heat transfer coefficient is primarily influenced by the heat flux, whereas the effect of mass flux and vapour quality is less significant. In forced convection region, heat is mainly transferred through the single phase annular liquid film and is carried away by the evaporation at an interface of liquid and vapour. In this region heat transfer coefficient mainly depends on mass velocity, vapour quality and heat flux. Peng and Wang [25] observed that flow boiling was reached to the fully developed nucleate boiling for wall temperature slightly higher than saturation temperature and was not affected by liquid velocity and subcooling.

Two phase heat transfer coefficient along the length of the microchannel was measured by Lee and Mudawar [61]. In their experiment, the quality of vapour was maintained by changing the mass flow rate of R134a. They suggested dividing the quality region into smaller interval for better estimate of heat transfer coefficient. They proposed three regions, $x_e < 0.05$ for nucleate boiling generated at low heat flux, $0.05 < x_e < 0.55$ for annular film evaporation generated at high heat flux and high mass flux and $x_e > 0.55$ for annular film evaporation generated at high heat flux and low mass flux. Whereas, Yen et al. [94] claimed through their experiments that nucleate boiling region remained dominate up to $x_e < 0.4$ in case of HCFC123 followed by convective boiling region. From the above discussion it can be concluded that vapour quality limit which determines the dominance of either nucleate boiling or convective boiling is dependent on individual fluid.

Kosar et al. [33] monitored variation of the two phase heat transfer coefficient with heat flux and mass flux. They observed that at low ($G = 41$ kg/m^2 s) and moderate ($G = 83$ and 166 kg/m^2 s) mass fluxes, two phase heat transfer coefficient dropped rapidly after critical heat flux condition due to complete dryout. However, at higher mass flux ($G = 302$ kg/m^2 s), two phase heat transfer coefficient decreased continuously from nucleate boiling to critical heat flux condition. They also observed large fluctuations in two phase heat transfer coefficient at low mass flux with exit vapour quality. They attributed it to the oscillatory flow pattern. Oscillatory flow pattern continuously shifted between confined bubble moving back and forth along the channel. Eventually, they concluded that nucleate boiling is dominant at low mass flux under all heat fluxes and moderate mass fluxes under low heat flux conditions. Whereas, for moderate mass fluxes under high heat flux and for high mass flux under all heat fluxes convective boiling is a dominant heat transfer mechanism. Schilder et al. [44] performed the experiments on circular glass tube ($D_h = 600$) using ethanol as working fluid. They observed that for single phase liquid flow, the measured Nusselt number approached the classical value for constant heat flux under Poiseuille flow ($Nu = 4.36$) at about 80% of the heated tube length. Based on two phase experiments they concluded that evaporation of thin liquid film covering the tube wall is dominating heat transfer mechanism. They further concluded that presence of wavy patterns on the film surface indicated the existence of shear force between the vapour and the liquid phase.

Steinke and Kandlikar [28] carried out flow boiling experiments on six rectangular microchannels with $D_h = 207$ μm using subcooled inlet conditions. They carried out experiments in heat flux range of 5–950 kW/m^2 and mass flux range of 157–1782 kg/m^2 s. They found that local heat transfer coefficient value was very high at very low vapour quality ($x_e \approx 0$), which they attributed formation of first bubble (carting maximum energy) on that location. Local flow boiling heat transfer coefficient decreased very sharply with increase in vapour quality irrespective of heat flux value, this was accredited in favour of rapid bubble growth. Yen et al. [94] and Sobierska et al. [37] also observed similar kind of trend in their studies as Steinke and Kandlikar [28]. Sobierska et al. [37] attributed the above to the following possible reasons; (i) partial dryout due to complete cross section filled by bubble, (ii) high pressure gradient associated with microchannels. Qu and Mudawar [26] also observed the same trend in their study and attributed it to appreciable droplet entrainment at the onset of annular flow regime. However, above reasons can not affect heat transfer characteristic in the vicinity of ONB, where vapour quality is very small. Retardation in local liquid phase velocity after ONB may be responsible for it. Park et al. [51] observed the same trend using FC-72 but for low heat flux ($q < 8.6$ kW/m^2) region only, they attributed it to the insufficient heat flux for generating active boiling in microchannels. At high heat flux values ($q > 8.6$ kW/m^2), the local heat transfer coefficient first increases up to certain vapour quality and then decreased. They also observed decreasing trend of local heat transfer coefficient with increase in mass flux at constant heat flux value, which they attributed to the possible dryout of the liquid film surrounding the elongated bubble and annular flow.

Bubble at nucleation site in microchannel is another aspect of important aspect of study considering various instabilities associated with it. Bubble at nucleation site in microchannel either grows linearly or exponentially (i.e. rapid bubble growth). Numerical study of the vapour bubble growth at nucleation site has been carried out by Zhuan and Wang [95]. However, detailed numerical bubble growth study is cumbersome and time consuming.

Furthermore, Rayleigh equation (used for determining the bubble growth in homogeneous superheated bulk medium [96–98]) predicts larger bubble growth rate than experimental value for heterogeneous bubble growth in microchannels [23,52]. Recently, Kadam et al. [99] developed simplified energy based model for prediction of the bubble growth at nucleation site in microchannel.

Yun et al. [36] carried out experiments to study the effects of mass flux, heat flux and saturation pressure on heat transfer characteristics. They observed that effect of mass flux, heat flux and saturation pressure on heat transfer coefficient was more significant after dryout vapour quality. After dryout vapour quality region, heat transfer coefficient increased with increase in mass flux, heat flux and saturation pressure respectively.

The variation of heat transfer coefficient of HFE 7100 with wall temperature and heat flux for different rectangular microchannels (W, H), (123.4, 304.9), (123.4, 526.9), (235.2, 576.8) and (259.9, 1041.3) was studied by Lee and Mudawar [85]. They concluded that smaller microchannel dimensions helped in improving the heat transfer characteristics by increasing mass velocity and wetted area. However, smaller width microchannels are more likely to face premature stability problems due to early transition from bubbly to slug flow. Balasubramanian et al. [46] compared the heat transfer coefficient in straight and expanding microchannel. They reported that heat transfer coefficient increased more rapidly with heat flux supplied in case of expanding microchannel as compared to straight microchannel. They attributed to it to the improved stability provided by expanding microchannel.

Study of Choo and Kim [100] was concentrated for finding the heat transfer characteristics of nonboiling two phase flow in microchannel. They observed the effect of microchannel hydraulic diameter on the heat transfer coefficient as shown in Fig. 8. When the channel diameter was smaller than about 235–260 μm, the two phase heat transfer was even lower than the single-phase case. They concluded that this may be due to the dominant effect of surface tension and liquid viscosity that prohibited the turbulent mixing in liquid film covering the wall. Furthermore, the transition channel diameter did not change once the gas Reynolds was increased beyond $Re = 300$. Experiments were performed with mixture of water and air on circular tubes of 140 μm–506 μm diameter under different flow rates of air and water.

Wang et al. [101] experimentally analysed the effect of channel inclination (rectangular microchannel $D_h = 825$) by carried out experiments at different heat flux (25, 37.5) and mass flux values (100, 200, 300). Experiments were performed at five different inclinations −90° (vertical downward), −45°, 0°, 45° and 90° (vertical upward). They observed that heat transfer coefficient increased by 30% at an inclination of 45° relative to horizontal orientation. They attributed the above to the two possible reasons (i) rise of distance between the bubble nose and contact surface brought the increase of velocity adjacent to the contact surface, (ii) concurrent nature of the inertia and buoyancy force. The heat transfer coefficient associated with vertical up ($\theta = 90°$) and horizontal ($\theta = 0°$) arrangements had almost same values due to the symmetric nature of the elongated bubble in both arrangements. For the vertical downward inclination heat transfer coefficient showed 50% lower value as compared to the inclination of 45° due to opposite direction of inertia and buoyancy forces.

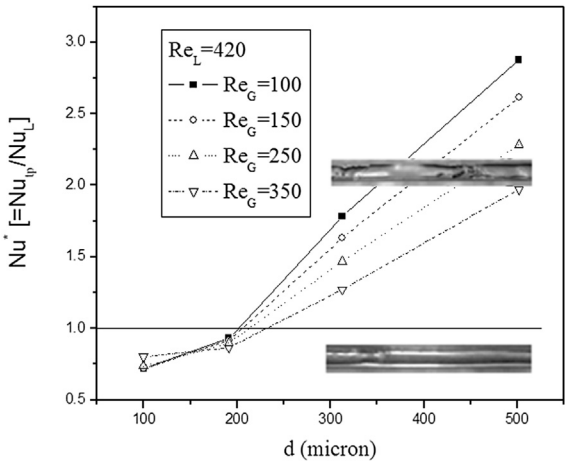

Fig. 8. The variation of the Nusselt number with channel hydraulic diameter for different Reynolds number (Choo and Kim [100]).

Lu and Pan [50] observed significant enhancement in heat transfer coefficient in microchannels with artificial nucleation sites, which facilitated bubble nucleation. Yen et al. [94] observed high heat transfer coefficient in case of square microchannel as compared to circular microchannel upto vapour quality of 0.4. This was attributed to square corners that acted as host for active nucleation sites. They reported similar heat transfer at high vapour quality for both cases. However, the trend may be opposite at annular flow regime, surface tension force intends to attenuate liquid film (on the wall) more effectively in case of square cross section. Resulting local dryout in case of square channel will reduce its heat transfer performance in comparison to circular channel.

Few correlations to predict heat transfer coefficient in single phase and two phase flow are reported in open literature. Tables 6 and 7 present details of these correlations for single phase and two phase respectively. These correlations for single phase and two phase heat transfer are plotted in Figs. 9 and 10, respectively against of experimental data of Koyuncuoglu et al. [104] for single phase and Qu and Mudawar [26] for two phase. Form Figs. 9 and 10, it can be concluded that existing heat transfer correlations are inconsistent and show large deviation in comparison to experimental data. This may be due to limited range of experimentation, difference in operating conditions, and difference in type of channel geometries used in these studies.

Therefore, still lot of efforts are needed so that generalized equations can be found for finding out heat transfer coefficient associated with single phase and two phase flow in microchannels.

5. Instability

Instability is also called as malfunctioning of the flow in microchannels. Instability in microchannel may cause several problems such as vibration, problems of system control, thermal fatigue and in extreme circumstances it may even be responsible for surface burnout. The well known instabilities associated with microchannels are flow reversal, pressure fluctuation, wall temperature fluctuation, flow maldistribution and Ledinegg instability. Out of above mention instabilities Ledinegg instability is static instability, whereas pressure fluctuation, wall temperature fluctuation and flow reversal are dynamic instabilities. A thorough understanding and determination of these associated instabilities are important.

Qi et al. [106] carried out experiments in order to study the two phase flow instabilities using liquid nitrogen as working fluid on two microtubes of diameter 1.042 and 1.931 mm. They observed repetitive regular oscillation of mass flux, pressure drop and wall temperature at ONB in both microtubes. These oscillations were referred as stable oscillation, as it remained stable, if system pressure, heat flux and outlet condition of the system did not change significantly. They explained that after ONB, many small bubbles nucleate, grow, detach from nucleation cavities and finally move along the flow in microtube. These small vapour bubbles entered

Table 6
Single phase heat transfer correlations.

Author and year	Channels geometry and fluid (W, H, D) μm	Operating parameter	Correlation
Wang and Peng [90]	Rectangular, $W = 200–800$, $H = 700$ Water and methanol	$P_{in} = 1$ bar, $T_{in,w} = 10–35$ °C, $T_{in,m} = 14–19$ °C, $Re = 1000–1500$.	$Nu = [0.00805Re^{4/5}Pr^{1/3}]$
Vidmar and Barker [102]	Circular, $D = 131$ Water	$P_s = 500–4500$ psi, $T_{in} = 23.4–31.4$ °C, $T_{out} = 74–163.1$ °C, $m = 1.510 \times 10^{-3} – 4.43 \times 10^{-3}$ kg/s	$Nu = 4.36$, for $Re < 2300$ $Nu = \left[\frac{(f/8)(Re-1000)Pr}{1+12.7(Pr^{2/3}-1)(f/8)^{1/2}}\right]$, for $2300 < Re < 20{,}000$ $Nu = \left[\frac{(f/8)RePr}{k_1+k_2(Pr^{2/3}-1)(f/8)^{1/2}}\right]$, for $10^4 < Re < 10^7$ $k_1 = 1+13.6(f_D/4)$, $k_2 = 11.7+1.8/Pr^{0.33}$ $Re = \frac{\rho V D_h}{\mu}$, $Pr = \frac{\mu C_p}{k}$ $f = \begin{cases} 0.079Re^{-0.25} & 4000 < Re < 20000 \\ 0.049Re^{-0.25} & 20000 < Re < 10^6 \\ [1.581\ln(Re)-3.28]^{-2} & 10000 < Re < 10^7 \end{cases}$ $\frac{1}{f_D^{0.5}} = 1.14 - 2log_{10}\left(\frac{e}{D_h}+\frac{9.35}{Ref_D^{0.5}}\right)$
Nacke et al. [103]	Rectangular, $W = 254$, $H = 762$ Water	$T_{in} = 24.4$ °C, $m = 0.001–0.0053$ kg/s.	$Nu = 3.66 + \frac{0.0668\left(\frac{D_h}{L}\right)RePr}{1+0.04\left[\left(\frac{D_h}{L}\right)RePr\right]^{2/3}}$, for Re <2300 and $Pr \geq 5$ $Nu = 1.86\left(\frac{RePr}{L/D_h}\right)^{1/3}\left(\frac{\mu_l}{\mu_{l,s}}\right)^{0.14}$, for Re <2300 and Pr <5
Koyuncuoglu et al. [104]	Rectangular, $W = 200$, $H = 50$ Water	$T_{in} = 24.4–25.1$ °C, $T_{out} = 70.7–96.8$ °C, $m = 2.91 \times 10^{-6} – 6.67 \times 10^{-6}$ kg/s	$Nu = (W/H)^{-0.053}(Re)^{0.782}(Pr)^{0.041}$

Table 7
Two phase heat transfer coefficient correlations.

Author and year	Channel geometry and fluid (W, H, D) μm	Operating condition	Correlation
Lee and Mudawar [61]	Rectangular, $W = 231$, $H = 713$ R134a	$P_{in} = 1.44–6.6$ bar, $q = 159–938$ kW/m^2, $G = 127–654$ kg/m^2 s, $x_{in} = 0.001–0.25$, $x_{out} = 0.49–$superheat	**For $x_e = 0–0.05$**, $h_{tp} = 3.856X^{0.267}h_{sp,l}$, where $X^2 = \frac{(dp/dz)_f}{(dp/dz)_g}$, $h_{sp,l} = Nu_3\frac{K_f}{D_h}$ $X_{vv} = \left(\frac{1-x_e}{x_e}\right)^{0.5}\left(\frac{\mu_f}{\mu_g}\right)^{0.5}\left(\frac{\nu_f}{\nu_g}\right)^{0.5}$ $X_{vt} = \left(\frac{f_f Re_g^{0.25}}{\mu_g}\right)^{0.5}\left(\frac{1-x_e}{x_e}\right)^{0.5}\left(\frac{\nu_f}{\nu_g}\right)^{0.5}$ $Nu_3 = 8.235(1-1.883\beta+3.767\beta^2-5.814\beta^3+5.361\beta^4-2\beta^5)$ **For $x_e = 0.05–0.5$** $h_{tp} = 436.48Bo^{0.522}We^{0.352}X^{0.665}h_{sp,l}$, where $h_{sp,l} = Nu_3(K_f/D_h)$ **For $x_e = 0.55–1$** $h_{tp} = \max\{108.6X^{1.667}h_{sp,g}, h_{sp,g}\}$ $h_{sp,g} = Nu_3\frac{K_g}{d_h}$ for laminar flow $h_{sp,g} = 0.023Re_g^{0.8}Pr_g^{0.4}$ for turbulent flow
Kosar et al. [33]	Rectangular, $W = 200$, $H = 264$, $L = 10$ mm Water	$q = 280–4450$ kW/m^2, $G = 41–302$ kg/m^2 s	$h_{tp} = 1.068(q'')^{0.64}$ Nucleate boiling, $h_{tp} = 4.068 \times 10^4(Re_l)^{0.12}(1-x_e)^{0.8}\left(\frac{1-x_e}{x_e}\right)^{0.02}$ Convective boiling
Bertsch et al. [105]	$D_h = 160–2920$	$T_{sat} = -194–90$ °C, $q = 4–1150$ kW/m^2, $G = 20–3000$ kg/m^2 s	$h = h_{nb}(1-x_e)+h_{cb}(1+80(x_e^2-x_e^6)e^{-0.6Co})$ $h_{nb} = 55P_r^{(0.12-0.2(\log_{10}R_p))}(-\log_{10}P_r)^{-0.55}M^{-0.5}q''^{0.67}$ $h_{cb} = h_{conv,\,l}(1-x_e)+h_{conv,\,v}x_e$, $h_{conv,\,L} = \left(3.66+\frac{0.0668D_h/LRe_lPr_l}{1+0.04[D_h/LRe_lPr_l]^{2/3}}\right)\frac{k_l}{D_h}$ $h_{conv,\,v} = \left(3.66+\frac{0.0668D_h/LRe_vPr_v}{1+0.04[D_h/LRe_vPr_v]^{2/3}}\right)\frac{k_v}{D_h}$, P_r = Inlet pressure/critical pressure = reduced pressure, $Co = \left[\frac{\sigma}{g(\rho_l-\rho_v)D_h^2}\right]^{0.5}$, $Re_l = \frac{GD_h}{\mu_l}$, $Re_v = \frac{GD_h}{\mu_v}$, $Pr_l = \frac{C_{p,\,l}\mu_l}{k_l}$, $Pr_v = \frac{C_{p,\,v}\mu_v}{k_v}$
Choo and Kim [100]	Circular, $D_h = 140–506$, water and air	$q = 340–950$ kW/m^2, $V_g = 1.24–40.1$ m/s, $V_l = 0.57–2.13$ m/s	$Nu_{tp} = 0.023Re_L^mPr_L^{0.4}F$, $F = CX^{-n}$, $m = 0.8-0.8[1+e^{(d^*-37)/7}]^{-1}$, $C = 2.94+358e^{-0.1d^*}$, $n = 0.7-0.8[1+e^{(d^*-41)/2}]^{-1}$, $d^* = d/\sqrt{\sigma/\rho g}$

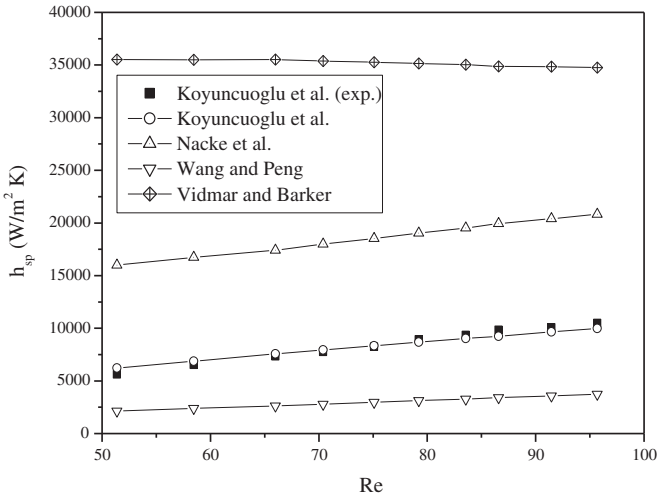

Fig. 9. Single phase heat transfer coefficient variation with Reynolds number.

and accumulated gradually into the outlet mixing chamber having diameter much larger than microtube that ultimately reduces bubble velocity. Hence, inertia force turned weaker and gravitational force magnitude increased significantly. Due to low vapour density these bubbles accumulated in upper part of outlet mixing chamber and formed vapour patch. This vapour patch temporarily blocked the mouth of outlet port. Thus, mass flux gradually decreased, which eventually resulted into increase in wall temperature and two phase vapour quality due to continual supply of heat flux. Higher exit vapour quality increased associated pressure drop. After discharge of the vapour patch, microchannel was again filled with fresh liquid nitrogen and the process repeated itself. Huh et al. [38] observed similar kind of oscillations in their study. They further concluded that pressure drop fluctuation and mass flux fluctuation remained in phase. Whereas, mass flux fluctuation and wall temperature fluctuation were exactly out of phase. They also observed that fluctuation period and fluctuation amplitude decreased with increase in mass flux and decrease in heat flux. Qu and Mudawar [86] carried out experiments on multiple parallel microchannels. They reported two types of instabilities, pressure drop oscillation and parallel channel instability associated with microchannels. Pressure drop oscillation produced fairly large

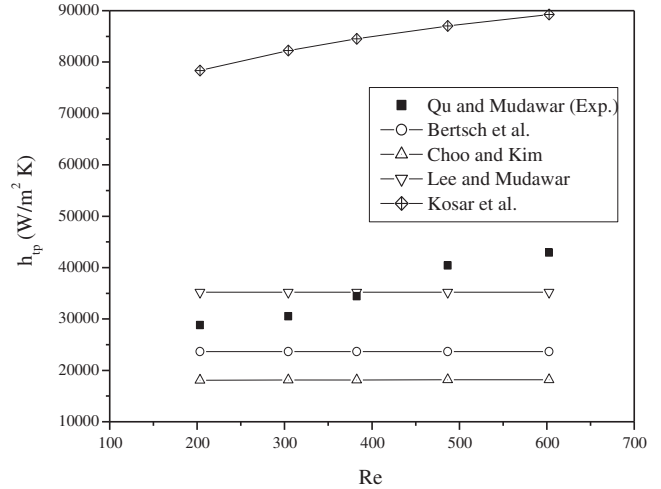

Fig. 10. Two phase heat transfer coefficient variation with Reynolds number.

periodic amplitude flow oscillation, which arose due to interaction between generated vapour and compressible volume coming from upstream direction. Whereas, parallel channels instability produced very mild flow oscillations resulting from density wave oscillation within each channels. They further reported that severe pressure drop can even lead to premature critical heat flux condition. Chang and Pan [107] concluded that large magnitude of the pressure drop oscillation may result into growing and shrinking of the bubble slug alternatively with flow reversal. Bogojevic et al. [108] carried out series of experiments on 40 parallel microchannels ($D_h = 194$) using water as working fluid. They observed that low inlet water temperature was subjected to higher magnitude of temperature oscillation. Whereas, high inlet water temperature promoted better flow distribution, which resulted into lower magnitude of temperature oscillation. Megahed [47] observed that microchannels were subjected to low magnitude of pressure and temperature fluctuation at high mass flux. Therefore, he concluded that flow becomes more stable at high mass flux. Balasubramanian et al. [46] observed that pressure fluctuation and wall temperature fluctuation were less severe in expanding microchannel than the straight microchannel under same operating conditions.

Flow reversal is another potential instability reported by several authors in which vapour slug flows back into inlet plenum. Qu and Mudawar [27] and Bergles and Kandlikar [109] observed that flow reversal occurs generally when CHF condition was approached. In the vicinity of CHF, rapid evaporation of the liquid caused bubble to expand in both upstream and downstream directions and form vapour slug. Kandlikar [110] concluded that location of the ONB decides the flow reversal. When nucleation occurred towards microchannel outlet (Fig. 11(a)), no flow reversal was observed. This was due to the fact that vapour pressure of liquid could not overcome inertia of incoming fluid. On the other hand, when nucleation was initiated near microchannel inlet, vapour bubble could easily overcome lower inertia of the incoming fluid. Thus, flow reversal was observed as shown in Fig. 11(b). Recently, Tuo and Hrnjak [111] studied the effect of the flow reversal on the performance of microchannel based evaporator of vapour compression system and concluded that it causes refrigerant flow maldistribution. They also concluded that local heat transfer coefficient may reduce because the vapour re-entrainment is likely to form a “dryout” bubble slug (without being surrounded by a thin liquid film). Kandlikar [110] mentioned that flow reversal could be avoided either by reducing the local liquid superheating at the ONB or by introducing pressure drop element at the entrance of each channel. Kaun and Kandlikar [112] performed experiments with inlet restrictors and observed that the flow become stable and flow reversal problem was reduced due to application of restrictors. Wang et al. [40] had also confirmed that the inlet restrictor helps in reducing flow reversal instability. Kuo and Peles [113] observed that the presence of reentrant cavities helped in reducing the pressure drop oscillation, parallel channel

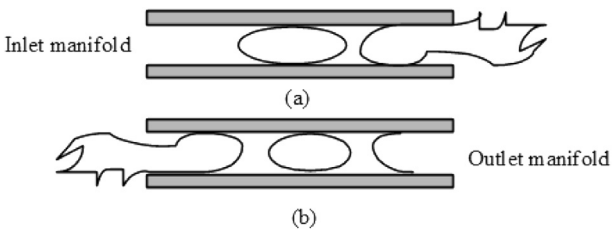

Fig. 11. Effect of nucleation location ((a) towards outlet, (b) towards) inlet on flow reversal (Kandlikar [110]).

instability and flow reversal instability by acting as host for active nucleation sites at much lower heat flux.

Xu et al. [114] and Liu et al. [115] experimentally demonstrated seed bubble generation method to mitigate flow instabilities (flow reversal, pressure drop oscillation and temperatures oscillation) associated with microchannels, which arises mainly due to strong thermal non equilibrium of liquid and vapour phase. Originally this idea was proposed by Thome and Dupont [116]. Seed bubbles are micron size bubble, generated on the set of microheaters, which were installed near to inlet port at the top wall of microchannels. These microheaters were driven by pulse voltage signal. When the voltage signal was on during pulse cycle, heating of microheaters generates seed bubble, Marangoni effect help in sticking of these seed bubbles at microheaters. As the signal turned off in the same pulse cycle, Marangoni effect become weak and shear force from the flowing liquid took away seed bubbles from microheaters surface. These seed bubble grow further soaking up energy from superheated liquid. At low frequency, these seed bubbles not only decreased oscillation amplitudes of pressure drop and temperature but also reduced oscillation cycle periods. At high frequency, these seed bubbles completely suppressed the flow instabilities. However, this method had not facilitated the subcooled liquid flow and vapour flow at high vapour mass quantities. Han and Shikazono [117] demonstrated air injection as a stabilization method for flow boiling in microtube using water as working fluid. They observed that pressure fluctuation and wall temperature fluctuation reduced significantly with increase in air injection flow rate.

Recently, Tuo and Hrnjak [118] proposed new vapour venting method to mitigate problem associated with flow reversal in microchannel evaporator. Proposed method provides 5% increase in cooling capacity and 3% increase in COP of air conditioning system.

In case of two phase flow in parallel microchannel heat sink, equal mass flow distribution to each microchannel is very important. In absence of properly design inlet/outlet header, microchannel heat sink is bound to face large amplitude fluctuation of pressure and temperature due to backward flow which eventually decrease the cooling capacity of heat sink and has to be obliged by running the system at moderate load. The headers which connect all microchannels in case multiple microchannel heat sink unavoidably introduce additional pressure drop due to contraction/expansion, friction and pressure loss/gain due to deceleration/acceleration [119]. This causes uneven pressure difference across each tube, resulting in unequal mass flow through each microchannel. Researchers have also suggested modification in of inlet/outlet header for removing flow maldistribution problem. Tonomura et al. [120] carried out CFD simulation to find optimum design of manifold for parallel microchannel heat sink. They observed that large outlet manifold provide uniform flow distribution. However, enlargement of outlet manifold increased dead volume inside microchannels. They also generated optimal shape header automatically (somewhat like trapezoidal header) by integration of optimization method with CFD simulation. Cho et al. [121] performed experiments on 33 straight and 33 diverging microchannels having rectangular as well as trapezoidal header. They observed that diverging microchannels with trapezoidal header gave more uniform flow distribution as compared to other configurations such as straight microchannel-rectangular header, straight microchannel-trapezoidal header and diverging microchannel-rectangular header. Cho et al. [122] carried out numerical simulation to obtained optimal header geometry which somewhat like trapezoidal in shape for two phase flow in the microchannel heat sink. Kumaraguruparan et al. [123] carried out numerical study on microchannel heat sink to investigate the causes of flow maldistribution. They observed that flow field in inlet header was non uniform due to occurrence of circulation zone at inlet of some channels which resulted into flow mal-distribution. Numerical results also showed that smaller width or depth or larger channel length turn flow distribution more uniform. Furthermore, flow mal-distribution problem aggravated at high flow rate or by the use of less viscous fluid. Tuo and Hrnjak [124] in their experimental study on microchannel evaporator (34 tubes) identified two types of fluid mal-distribution: quality induced mal-distribution and header pressure drop induced mal-distribution. They used flash gas bypass method to mitigate problem of the quality induced mal-distribution. They also observed that increase in outer header diameter resulted into uniform flow rate in each microctube. Szczukiewicz et al. [125] concluded through their visual observation on sixty seven rectangular microchannels (100, 100) evaporator that introduction of the inlet orifice successfully suppressed flow instability, vapour back flow and significantly improved flow uniformity across microchannel.

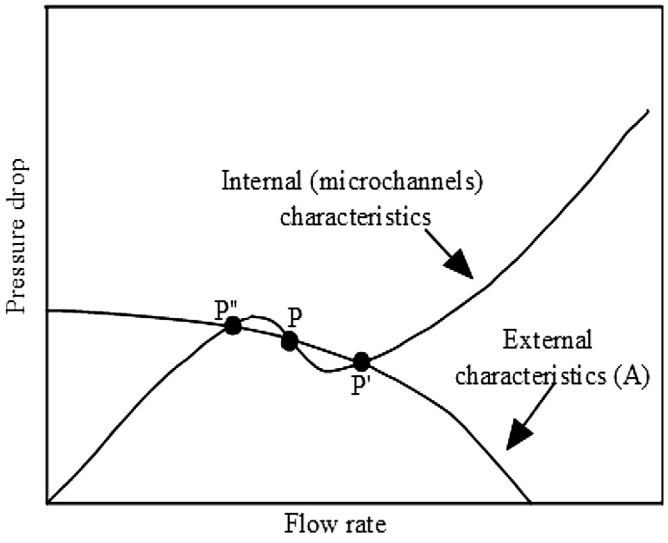

Fig. 12. Ledinegg instability (Kakac and Bon [97]).

Study of Ledinegg instability is helpful to avoid malfunctioning of the pump used in microchannels heat sink loop. As per Kakac and Bon [126], Ledinegg instability is due to sudden variation in flow rate to a lower value. It is explained through pressure drop verses mass flow rate characteristics reported by Kakac and Bon [126] in Fig. 12. It occurred when slope of the channels demand curve (internal characteristics curve) is negative and steeper than the loop supply curve (external characteristics curve, A) and under multiple interaction of this both curves (P, P', P''). A slight variation in flow rate to the lower side result in more pressure drop is required to sustain the flow available from external curve. Zhang et al. [127] studied Ledinegg instability in microchannels and proposed ways to avoid this instability as having less number of channels, increased system pressure, lower heat flux, low subcooling and short channels.

6. Concluding remark

Following are conclusive remarks and suggestions of current work:

i. Flow visualization study is very important as it gives an insight of the heat transfer and the pressure drop characteristics. Lot of flow visualization studies have been carried out on microchannels. However, unlike conventional channels, flow regimes are not well accepted yet for

microchannels. Phenomena like bubble suppression, bubble circulation, bubble nucleation inside thin liquid film, bubble condensation, and their effect on flow regimes are not well studied yet. Hence, unusual states such as absence of bubbly flow, swirling pattern in churn flow and liquid bridges in slug–annular flow have been reported in different research works.

ii. Majority of the microchannel research work in the last two decades had been oriented for better understanding of mechanism involved in heat transfer. Current heat transfer correlations comparative study shows that still lot of efforts are needed for setting up generalized heat transfer correlations for microchannels. Limited range of experimentation, difference in operating conditions, and channel geometries could be possibly responsible for that. Future research will certainly focus more on finding suitable heat transfer augmentation techniques by choosing among from conventionally proven methods e.g. extended surfaces, artificial nucleation sites, surfactants, artificial surface roughness, nanofluid etc.

iii. Various instabilities associated with two phase flow are the main constraints limiting the application of microchannels. Few suggestions have been made in order to avoid instabilities such as flow reversal (reducing liquid superheating at ONB, throttling at inlet of microchannels and re-entrant cavities), Pressure and temperature oscillations (operating at high mass fluxes, and expanding microchannels) and Ledinegg instability (increased system pressure, lower heat flux, low subcooling and short channels). More studies are needed in this direction such as novel design can be devised free from major instabilities.

iv. Majority of the studies have been carried out on rectangular microchannels or microtubes. Very few studies have been carried out on other cross sections like trapezoidal, V-shape, hexagonal etc. It would be interesting to know, what is the effect of channel geometry on heat transfer characteristics and especially on instabilities. Moreover, refrigerant like R600a and R290 (with low ozone layer depletion potential) have not been explored as working fluid in microchannels.

v. The bubble dynamics (i.e. such as vapour bubble nucleation, growth, departure from nucleation site and its motion along the flow) governs the two phase heat transfer, pressure drop characteristics and possibly associated instabilities also. Use of conventional channel theory is ambiguous for this task. Detailed numerical study of the each stage will be helpful in accurately predicting heat transfer and pressure drop characteristics under wide range of operating conditions.

Nomenclature

A	channel cross section (m^2)
A_p	plenum cross section area (m^2)
C_c	contraction coefficient
Co	confinement number
C_p	specific heat (J/kg K)
C_{vv}	two phase parameter based on laminar liquid–laminar vapour flow
C_{vt}	two phase parameter based on laminar liquid–turbulent vapour flow
D_h	hydraulic diameter (m)
e	surface roughness (m)
f	fanning friction factor
f_{app}	apparent friction factor for developing single-phase liquid flow
f_D	Darcy friction factor
G	mass flux (kg/m^2 s)
H	microchannel width (μm)
h	heat transfer coefficient (W/m^2 K)
h_{fg}	latent heat (kJ/kg)
K	thermal conductivity (W/m K), coefficient
K_c	contraction coefficient
K_∞	Hegenbach factor
L	channel length (m)
M	molecular mass of the fluid (kg/kmol)
m	mass flow rate (kg/s)
N	number of microchannel
Nu	Nusselt number
ΔP	pressure drop (Pa)
Pr	Prandtl number
P_r	reduced pressure (inlet pressure/saturation pressure)
Re	Reynolds number
R_p	surface roughness parameter (μm)
T	temperature (°C)
Q_{net}	net heat supplied (w).
q''	effective heat supplied (W/m^2)
u	mean velocity in port (m/s)
u_{ch}	mean velocity in microchannel (m/s)
V	velocity (m/s)
v	specific volume (m^3/kg)
v_{fg}	difference in specific volume of saturated liquid and vapour
W	channel width (μm)
We	Weber number
X	Martinelli parameter
x_e	thermodynamic equilibrium quality
x_L	equilibrium quality at end of the heated length

Greek

α_{in}	inlet void fraction
α_{out}	outlet void fraction
β	aspect ratio
θ	static contact angle (°)
μ	dynamic viscosity (Pa-s)
σ_c	contraction area ratio
σ_e	expansion area ratio

Subscript

1	deep plenum.
2	shallow plenum
3	three sided wall heating
a	acceleration
c	contraction
cb	convective boiling
conv	convective
dev	developing region
dyn	dynamic
e	expansion
f	friction, fluid
fdev	fully developed region
g	gas
i	inlet
l	liquid
nb	nucleate boiling
nh	non heating
out	outlet
s	solid surface
sat	saturated
sub	subcooled
sp	single phase
T	total

tp two phase
vt laminar liquid–turbulent vapour flow
vv laminar liquid–laminar vapour flow

References

[1] I. Mudawar, Two-phase microchannel heat sink: theory, application and limitation, J. Electron. Packag. 133 (2002), http://dx.doi.org/10.1115/1.4005300.
[2] R. Ali, Phase Change Phenomena during Fluid Flow in Micro Channels (Doctoral Thesis), Royal Institute of Technology, Stockholm, Sweden, 2010.
[3] E. Pop, K.E. Goodson, Thermal phenomena in nanoscale transistors, J. Electron. Packag. 128 (2006) 102–108.
[4] R.J. Phillips, Microchannel heat sinks, Linc. Lab. J. 1 (1988) 31–47.
[5] J. Lee, I. Mudawar, Fluid flow and heat transfer characteristics of low temperature two-phase micro-channel heat sink – part1: experimental methods and flow visualization results, Int. J. Heat Mass Transf. 51 (2008) 4315–4326.
[6] R.D. Boyd, Subcooled flow boiling critical heat flux and its application to fusion energy components. Part 1. A review of fundamentals of CHF and related data base, Fusion Technol. 7 (1985) 7–30.
[7] J. Lee, I. Mudawar, Low-temperature two-phase microchannel cooling for high heat-flux thermal management of defence electronics, IEEE Trans. Compon. Packag. Technol. 32 (2009) 453–465.
[8] S.G. Kandlikar, High flux heat removal with microchannels- A roadmap of challenges and opportunities, Heat Transf. Eng. 26 (2005) 5–14.
[9] D.B. Tuckerman, R.F.W. Pease, High-performance heat sinking for VLSI, IEEE Electron Device Lett. 2 (1981) 126–129.
[10] R.W. Keyes, Heat transfer in forced convection through fins, IEEE Trans. Electron Devices 311 (1984) 1218–1221.
[11] I.J. Missaggia, J.N. Walpole, Z.L. Liau, R.J. Phillips, Microchannel heat sinks for two-dimensional high-power-density diode laser arrays, IEEE J. Quantum Electron. 25 (1989) 1988–1992.
[12] S.G. Kandlikar, W.J. Grande, Evolution of microchannel flow passages––thermohydraulic performance and fabrication technology, in: ASME International Mechanical Engineering Congress & Exposition, November 17–22, New Orleans, Louisiana, 2002.
[13] S.G. Kandlikar, W.J. Grande, Evolution of microchannel flow passage thermohydraulic performance and fabrication technology, Heat Transf. Eng. 24 (2003) 3–17.
[14] S.S. Mehendale, A.M. Jacobi, R.K. Shah, Fluid flow and heat transfer at micro- and meso-scales with applications to heat exchanger design, Appl. Mech. Rev. 53 (2000) 175–193.
[15] K. Cornwell, P.A. Kew, Boiling in Small Parallel Channels, Energy Efficiency in Process Technology Elsevier, 1993, pp. 624–638 (Chap. 7).
[16] P. Kew, K. Cornwell, Correlation for prediction of boiling heat transfer in small diameter channel, J. Therm. Eng. 17 (1997) 705–715.
[17] I. Papautsky, J. Brazzle, H. Swerdlow, A.B. Frazier, A low-temperature IC compatible process for fabricating surface-micromachined metallic microchannels, J. Microelectromech. Syst. 7 (1998) 267–273.
[18] P.S. Lee, S.V. Garimella, D. Liu, Investigation of heat transfer in rectangular microchannels, Int. J. Heat Mass Transf. 48 (2005) 1688–1704.
[19] H.Y. Wu, P. Cheng, Condensation flow pattern in silicon microchannels, Int. J. Heat Mass Transf. 48 (2005) 2186–2197.
[20] F. Mei, P.R. Parida, J. Jiang, W.J. Meng, S.V. Ekkad, Fabrication, assembly, and testing of Cu- and Al- based microchannel heat exchanger, J. Microelectromech. Syst. 17 (2008) 869–881.
[21] J. Wu, M. Shi, Y. Chen, X. Li, Visualization study of steam condensation in wide rectangular silicon microchannels, Int. J. Therm. Sci. 49 (2010) 922–930.
[22] T. Chen, S.V. Garimella, Local heat transfer distribution and effect of instabilities during flow boiling in a silicon microchannel heat sink, Int. J. Heat Mass Transf. 54 (2011) 3179–3190.
[23] J.Y. Lee, M.H. Kim, M. Kaviany, S.Y. Son, Bubble nucleation in microchannel flow boiling using single artificial cavity, Int. J. Heat Mass Transf. 54 (2011) 5139–5148.
[24] D.J. Hwang, T.Y. Choi, C.P. Grigoropoulos, Liquid assisted femtosecond laser drilling of straight and three-dimensional micro-channels in glass, Appl. Phys. A 79 (2004) 605–612.
[25] X.F. Peng, B.X. Wang, Forced convection and flow boiling heat transfer for liquid flowing through microchannels, Int. J. Heat Transf. 36 (1993) 3421–3427.
[26] W. Qu, I. Mudawar, Flow boiling heat transfer in two-phase micro-channel heat sinks––I. Experimental investigation and assessment of correlation methods, Int. J. Heat Mass Transf. 46 (2003) 2755–2771.
[27] W. Qu, I. Mudawar, Measurement and correlation of critical heat flux in two-phase micro-channel heat sinks, Int. J. Heat Mass Transf. 47 (2004) 2045–2059.
[28] M.E. Steinke, S.G. Kandlikar, An experimental investigation of flow boiling characteristics of water in parallel microchannels, J. Heat Transf. 126 (2004) 518–526.
[29] J.W. Coleman, P.E. Krause, two phase pressure losses of R134a in microchannel tube headers with large free flow area ratios, Exp. Therm. Fluid Sci. 28 (2004) 123–130.
[30] P.C. Lee, F.G. Tseng, C. Pan, Bubble dynamics in microchannels. Part I: single microchannel, Int. J. Heat Mass Transf. 47 (2004) 5575–5589.
[31] H.Y. Li, F.G. Tseng, C. Pan, Bubble dynamics in microchannels. Part II: two parallel microchannels, Int. J. Heat Mass Transf. 47 (2004) 5591–5601.
[32] J. Lee, I. Mudawar, Two-phase flow in high-heat-flux micro-channel heat sink for refrigeration cooling applications: part I––pressure drop characteristics, Int. J. Heat Mass Transf. 48 (2005) 928–940.
[33] A. Kosar, C.J. Kuo, Y. Peles, Boiling heat transfer in rectangular microchannels with reentrant cavities, Int. J. Heat Mass Transf. 48 (2005) 4867–4886.
[34] Z.Y. Ling, J.N. Ding, J.C. Yang, Y. Liu, Z. Fan, P. Yang, Z.W. Zhuang, Experimental study of flow characteristics of distilled water under pressure driven in microchannel, in: Proc. 1st IEEE Int. Conference on Nano/Micro Engineered and Molecular Systems, Zhuhai, China, 2006, pp. 182–186.
[35] T. Chen, S.V. Garimella, Measurements and high-speed visualizations of flow boiling of a dielectric fluid in a silicon microchannel heat sink, Int. J. Multiphase Flow 32 (2006) 957–971.
[36] R. Yun, J.Y. Heo, Y. Kim, Evaporative heat transfer and pressure drop of R410A in microchannels, Int. J. Refrig. 29 (2006) 92–100.
[37] E. Sobierska, R. Kulenovic, R. Mertz, M. Groll, experimental results of flow boiling of water in a vertical microchannel, Exp. Therm. Fluid Sci. 31 (2006) 111–119.
[38] C. Huh, J. Kim, M.H. Kim, Flow pattern transition instability during flow boiling in a single microchannel, Int. J. Heat Mass Transf. 50 (2007) 1049–1060.
[39] S.L. Qi, P. Zhang, R.Z. Wang, L.X. Xu, Single-phase pressure drop and heat transfer characteristics of turbulent liquid nitrogen flow in micro-tubes, Int. J. Heat Mass Transf. 50 (2007) 1993–2001.
[40] G. Wang, P. Cheng, A.E. Bergles, Effects of inlet/outlet configurations on flow boiling instability in parallel microchannels, Int. J. Heat Mass Transf. 51 (2008) 2267–2281.
[41] B. Agostini, R. Revellin, J.R. Thome, Elongated bubbles in microchannels. Part I: experimental study and modeling of elongated bubble velocity, Int. J. Multiphase Flow 34 (2008) 590–601.
[42] S.G. Singh, A. Kulkarni, S.P. Duttagupta, B.P. Puranik, A. Agrawal, Impact of aspect ratio on flow boiling of water in rectangular microchannels, Exp. Therm. Fluid Sci. 33 (2008) 153–160.
[43] O.B. Ergu, O.N. Sara, S. Yapici, M.E. Arzutug, Pressure drop and point mass transfer in a rectangular microchannel, Int. Commun. Heat Mass Transf. 36 (2009) 618–623.
[44] B. Schilder, S.Y.C. Man, N. Kasagi, S. Hardt, P. Stephan, Flow visualization and local measurement of forced convection heat transfer in a microtube, J. Heat Transf. 132 (2010), http://dx.doi.org/10.1115/1.4000046.
[45] S. Krishnamurthy, Y. Peles, Flow boiling heat transfer on micro pin fins entrenched in a microchannel, J. Heat Transf. 132 (2010), http://dx.doi.org/10.1115/1.4000878.
[46] K. Balasubramanian, P.S. Lee, L.W. Jin, S.K. Chou, C.J. Teo, S. Gao, Experimental investigations of flow boiling heat transfer and pressure drop in straight and expanding microchannels – a comparative study, Int. J. Therm. Sci. 50 (2011) 241–2421.
[47] A. Megahed, Experimental investigation flow boiling characteristics in a cross-linked microchannel heat sink, Int. J. Multiphase Flow 37 (2011) 380–393.
[48] S. Barlak, S. Yapici, O.N. Sara, Experimental investigation of pressure drop and friction factor for water flow in microtubes, Int. J. Therm. Sci. 50 (2011) 361–368.
[49] Z.J. Edel, A. Mukherjee, Experimental investigation of vapor bubble growth during flow boiling in a microchannel, Int. J. Multiphase Flow 37 (2011) 1257–1265.
[50] C.T. Lu, C. Pan, Convective boiling in a parallel microchannel heat sink with a diverging cross section and artificial nucleation sites, Exp. Therm. Fluid Sci. 35 (2011) 810–815.
[51] C.Y. Park, Y. Jang, B. Kim, Y. Kim, Flow boiling heat transfer coefficients and pressure drop of FC-72 in microchannels, Int. J. Multiphase Flow 39 (2012) 45–54.
[52] J.R. Thome, Engineering Data Book III, Wolverine Tube Inc., 2004 (Chap. 12).
[53] J. Pfahler, J. Harley, H. Bau, J. Zemel, Liquid transport in micron and submicron channels, Sens. Actuators 22 (1990) 431–434.
[54] A. Megahed, I. Hassan, Two-phase pressure drop and flow visualization of FC-72 in a silicon microchannel heat sink, Int. J. Heat Fluid Flow 30 (2009) 1171–1182.
[55] P. Zhang, X. Fu, Two-phase flow characteristics of liquid nitrogen in vertically upward 0.5 and 1.0 mm micro-tubes: visualization studies, Cryogenics 49 (2009) 565–575.
[56] A. Kawahara, M. Sadatomi, K. Nei, H. Matsuo, Experimental study on bubble velocity, void fraction and pressure drop for gas–liquid two-phase flow in a circular microchannel, Int. J. Heat Fluid Flow 30 (2009) 831–841.
[57] C. Choi, M. Kim, Flow pattern based correlations of two-phase pressure drop in rectangular microchannels, Int. J. Heat Fluid Flow 32 (2011) 1199–1207.
[58] C.W. Choi, D.I. Yu, M.H. Kim, Adiabatic two-phase flow in rectangular microchannels with different aspect ratios: part I – flow pattern, pressure drop and void fraction, Int. J. Heat Mass Transf. 54 (2011) 616–624.
[59] K.E. Kasza, T. Didascalou, M.W. Wambsganss, Microscale flow visualization of nucleate boiling in small channels: mechanisms influencing heat transfer, in: Proc. International Conference on Compact Heat Exchanges for the Process Industries, Begell House Inc., New York, 1997, pp. 343–352.

[60] P.M.Y. Chung, M. Kawaji, The effect of channel diameter on adiabatic two-phase flow characteristics in microchannels, Int. J. Multiphase Flow 30 (2004) 735–761.
[61] J. Lee, I. Mudawar, Two-phase flow in high-heat-flux micro-channel heat sink for refrigeration cooling applications: part II—heat transfer characteristics, Int. J. Heat Mass Transf. 48 (2005) 941–955.
[62] M.N. Kashid, I. Gerlach, S. Goetz, J. Franzke, J.F. Acker, F. Platte, D.W. Agar, S. Turek, Internal circulation within the liquid slugs of liquid–liquid slug flow capillary microreactor, Ind. Eng. Chem. Res. 44 (2005) 5003–5010.
[63] J. Barber, D. Brutin, K. Sefiane, L. Tadrist, Bubble confinement in flow boiling of FC-72 in a "rectangular" microchannel of high aspect ratio, Exp. Therm. Fluid Sci. 34 (2010) 1375–1388.
[64] M.P. David, J.E. Steinbrenner, J. Miler, K.E. Goodson, Adiabatic and diabatic two-phase venting flow in a microchannel, Int. J. Multiphase Flow 37 (2011) 1135–1146.
[65] G.F. Hewitt, D.N. Roberts, Studies of Two-phase Flow Patterns by Simultaneous X-ray and Flash Photography, Atomic Energy Research Establishment, 1969. Harwell, Report No. AERE-M 2159.
[66] Y. Taitel, A.E. Dukler, A model for predicting flow regime transitions in horizontal and near horizontal gas-liquid flow, AIChE J. 22 (1976) 47–55.
[67] N. Kattan, J.R. Thome, D. Favrat, Flow boiling in horizontal tubes—part I: development of a diabatic two-phase flow pattern map, J. Heat Transf. 120 (1998) 140–147.
[68] N. Kattan, J.R. Thome, D. Favrat, Flow boiling in horizontal tubes—part II: new heat transfer data for five refrigerants, J. Heat Transf. 120 (1998) 148–155.
[69] N. Kattan, J.R. Thome, D. Favrat, Flow boiling in horizontal tubes—part III: development of a new heat transfer model based on flow patterns, J. Heat Transf. 120 (1998) 156–165.
[70] K.A. Triplett, S.M. Ghiaasiaan, S.I. Abdel-Khalik, D.L. Sadowski, Gas–liquid two-phase flow in microchannels part I: two-phase flow patterns, Int. J. Multiphase Flow 25 (1999) 377–394.
[71] T. Harirchian, S.V. Garimella, A comprehensive flow regime map for microchannel flow boiling with quantitative transition criteria, Int. J. Heat Mass Transf. 53 (2010) 2694–2702.
[72] A. Sur, D. Liu, Adiabatic air-water two-phase flow in circular microchannels, Int. J. Therm. Sci. 53 (2012) 18–34.
[73] D. Liu, P.S. Lee, S.V. Garimella, Prediction of the onset of nucleate boiling in microchannels flow, Int. J. Heat Mass Transf. 48 (2005) 5134–5149.
[74] Y.Y. Hsu, On the size range of active nucleation cavities on a heating surface, J. Heat Transf. 84 (1962) 207–216.
[75] S. Meder, Study on Bubble Growth Rate in a Single Microchannel Heat Exchanger with High-speed CMOS-camera (Master Thesis), Swiss Federal Institute Of Technology, Zurich And Stanford University California, 2007.
[76] D. Bogojevic, K. Sefiane, D. Duursma, A.J. Walton, Bubble dynamics and flow boiling instabilities in microchannels, Int. J. Heat Mass Transf. 58 (2013) 663–675.
[77] M. Lee, Y.Y. Wong, M. Wong, Y. Zohar, Size and shape effects on two-phase flow patterns in microchannel forced convection boiling, J. Micromech. Microeng. 13 (2003) 155–164.
[78] X. Fu, P. Zhang, C.J. Huang, R.Z. Wang, Bubble growth, departure and the following flow pattern evolution during flow boiling in a mini-tube, Int. J. Heat Mass Transf. 53 (2010) 4819–4831.
[79] S. Gedupudi, Y.Q. Zu, T.G. Karayiannis, D.B.R. Kenning, Y.Y. Yan, Confined bubble growth during flow boiling in a mini/micro-channel of rectangular cross-section part I: experiments and 1-D modeling, Int. J. Therm. Sci. 50 (2011) 250–266.
[80] L. Yin, L. Jia, P. Guan, F. Liu, An experimental investigation on the confined and elongated bubbles in subcooled flow boiling in a single microchannel, J. Therm. Sci. 21 (2012) 549–556.
[81] H. Tuo, P. Hrnjak, Visualization and measurement of periodic reverse flow and boiling fluctuations in a microchannel evaporator of an air-conditioning system, Int. J. Heat Mass Transf. 71 (2014) 639–652.
[82] W. Qu, I. Mudawar, Experimental and numerical study of pressure drop and heat transfer in a single-phase micro-channel heat sink, Int. J. Heat Mass Transf. 45 (2002) 2549–2565.
[83] M. Akbari, D. Sinton, M. Bahrami, Pressure drop in rectangular microchannels as compared with theory based on arbitrary cross section, J. Fluids Eng. 131 (2009), http://dx.doi.org/10.1115/1.3077143.
[84] W. Peiyi, W.A. Little, Measurement of friction factors for the flow of gases in very fine channels used for microminiature Joule–Thomson refrigerator, Cryogenics 23 (1983) 73–277.
[85] J. Lee, I. Mudawar, Fluid flow and heat transfer characteristics of low temperature two-phase micro-channel heat sinks – part 2. subcooled boiling pressure drop and heat transfer, Int. J. Heat Mass Transf. 51 (2008) 4327–4341.
[86] W. Qu, I. Mudawar, Measurement and prediction of pressure drop in two-phase micro-channel heat sinks, Int. J. Heat Mass Transf. 46 (2003) 2737–2753.
[87] P.S. Lee, S.V. Garimella, Saturated flow boiling heat transfer and pressure drop in silicon microchannel arrays, Int. J. Heat Mass Transf. 51 (2008) 789–806.
[88] H.T. Phan, N. Caney, P. Marty, S. Colasson, J. Gavillet, Flow boiling of water in a minichannel: the effects of surface wettability on two-phase pressure drop, J. Therm. Eng. 31 (2011) 1894–1905.
[89] M.B. Bowers, I. Mudawar, High flux boiling in low flow rate, low pressure drop mini-channel and microchannel heat sink, Int. J. Heat Mass Transf. 37 (1994) 331–332.
[90] B.X. Wang, X.F. Peng, Experimental investigation on liquid forced convection heat transfer through microchannels, Int. J. Heat Transf. 37 (1994) 73–82.
[91] H. Herwig, S.P. Mahulikar, Variable property effects in single-phase incompressible flows through microchannels, Int. J. Therm. Sci. 45 (2006) 977–981.
[92] Y. Sui, P.S. Lee, C.J. Teo, An experimental study of flow friction and heat transfer in wavy microchannels with rectangular cross section, Int. J. Therm. Sci. 50 (2011) 2473–2482.
[93] J.G. Collier, J.R. Thome, Convective Boiling and Condensation, third ed., Oxford University Press, Oxford, 1994.
[94] T.H. Yen, M. Shoji, F. Takemura, Y. Suzuki, N. Kasagi, Visualization of convective boiling heat transfer in single microchannels with different shaped cross-sections, Int. J. Heat Mass Transf. 49 (2006) 3884–3894.
[95] R. Zhuan, W. Wang, Simulation on nucleate boiling in microchannel, Int. J. Heat Mass Transf. 53 (2010) 502–512.
[96] M.S. Plesset, S.A. Zwick, Growth of vapor bubbles in superheated liquids, Appl. Phys. 25 (1954) 493–500.
[97] H.K. Forster, N. Zuber, Growth of a vapor bubbles in superheated liquid, Appl. Phys. 25 (1954) 474–478.
[98] M.S. Plesset, A. Prosperetti, Bubble dynamics and cavitation, Annu. Rev. Fluid Mech. 9 (1977) 145–185.
[99] S.T. Kadam, R. Kumar, K. Baghel, Simplified model for prediction of bubble growth in microchannels, J. Heat Transf. 136 (2014), http://dx.doi.org/10.1115/1.4026609.
[100] K. Choo, S.J. Kim, Heat transfer and fluid flow characteristics of nonboiling two-phase flow in microchannels, J. Heat Transf. 133 (2011), http://dx.doi.org/10.1115/1.4004208.
[101] C.C. Wang, W.J. Chang, C.D. Dai, Y.T. Lin, K.S. Yang, Effect of inclination on the convective boiling performance of a microchannel heat sink using HFE-7100, Exp. Therm. Fluid Sci. 36 (2012) 143–148.
[102] R.J. Vidmar, R.J. Barker, Microchannel cooling for a high-energy particle transmission window, an RF transmission window, and VLSI heat dissipation, IEEE Trans. Plasma Sci. 26 (1998) 1031–1043.
[103] R. Nacke, B. Northcutt, I. Mudawar, Theory and experimental validation of cross-flow micro-channel heat exchanger module with reference to high Mach aircraft gas turbine engines, Int. J. Heat Mass Transf. 54 (2011) 1224–1235.
[104] A. Koyuncuoglu, R. Jafari, T.O. Ozyurt, H. Kulah, Heat transfer and pressure drop experiments on CMOS compatible microchannel heat sinks for monolithic chip cooling applications, Int. J. Therm. Sci. 56 (2012) 77–85.
[105] S.S. Bertsch, E.A. Groll, S.V. Garimella, A composite heat transfer correlation for saturated flow boiling in small channels, Int. J. Heat Mass Transf. 52 (2009) 2110–2118.
[106] S.L. Qi, P. Zhang, R.Z. Wang, L.X. Xu, Flow boiling of liquid nitrogen in microtubes: part I – the onset of nucleate boiling, two-phase flow instability and two-phase flow pressure drop, Int. J. Heat Mass Transf. 50 (2007) 4999–5016.
[107] K.H. Chang, C. Pan, Two-phase flow instability for boiling in a microchannel heat sink, Int. J. Heat Mass Transf. 50 (2007) 2078–2088.
[108] D. Bogojevic, K. Sefiane, A.J. Walton, H. Lin, G. Cummins, Two-phase flow instabilities in a silicon microchannels heat sink, Int. J. Heat Fluid Flow 30 (2009) 854–867.
[109] A.E. Bergles, S.G. Kandlikar, On the nature of critical heat flux in microchannels, J. Heat Transf. 127 (2005) 101–107.
[110] S.G. Kandlikar, Nucleation characteristics and stability considerations during flow boiling in microchannels, Exp. Therm. Fluid Sci. 30 (2006) 441–447.
[111] H. Tuo, P. Hrnjak, Periodical reverse flow and boiling fluctuations in a microchannel evaporator of an air-conditioning system, Int. J. Refrig. 36 (2013) 1263–1275.
[112] W.K. Kuan, S.G. Kandlikar, Experimental study on the effect of stabilization on flow boiling heat transfer in microchannels, Heat Transf. Eng. 28 (2007) 746–752.
[113] C.J. Kuo, Y. Peles, Flow boiling instabilities in microchannels and means or mitigation by reentrant cavities, J. Heat Transf. 130 (2008), http://dx.doi.org/10.1115/1.2908431.
[114] J. Xu, G. Liu, W. Zhang, Q. Li, B. Wang, Seed bubbles stabilize flow and heat transfer in parallel microchannels, Int. J. Multiphase Flow 35 (2009) 773–790.
[115] G. Liu, J. Xu, Y. Yang, W. Zhang, Active control of flow and heat transfer in silicon microchannels, J. Micromech. Microeng. 20 (2010) 1–16.
[116] J.R. Thome, V. Dupont, Heat Transfer Assembly, European Patent EP 1779052 B1, 2007.
[117] Y. Han, N. Shikazono, Stabilization of flow boiling in a micro tube with air injection, Exp. Therm. Fluid Sci. 35 (2011) 1255–1264.
[118] H. Tuo, P. Hrnjak, New approach to improve performance by venting periodic reverse vapor flow in microchannel evaporator, Int. J. Refrig. 36 (2013) 2187–2195.
[119] J.M. Yin, C.W. Bullard, P.S. Hrnjak, Single phase pressure drop measurements in a microchannel heat exchanger, Heat Transf. Eng. 23 (2002) 1–10.
[120] O. Tonomura, S. Tanaka, M. Noda, M. Kano, S. Hasebe, I. Hashimoto, CFD-based optimal design of manifold in plate-fin microdevices, Chem. Eng. J. 101 (2004) 397–402.

[121] E.S. Cho, J.W. Choi, J.S. Yoon, M.S. Kim, Experimental study on microchannel heat sinks considering mass flow distribution with non-uniform heat flux conditions, Int. J. Heat Mass Transf. 53 (2010) 2159–2168.
[122] E.S. Cho, J.W. Choi, J.S. Yoon, M.S. Kim, Modeling and simulation on the mass flow distribution in microchannel heat sinks with non uniform heat flux conditions, Int. J. Heat Mass Transf. 53 (2010) 1341–1348.
[123] G. Kumaraguruparan, R.M. Kumaran, T. Sornakumar, T. Sundararajan, A numerical and experimental investigation of flow maldistribution in a microchannel heat sink, Int. Commun. Heat Mass Transf. 380 (2011) 1349–1353.
[124] H. Tuo, P. Hrnjak, Effect of the header pressure drop induced flow maldistribution on the microchannel evaporator performance, Int. J. Refrig. 36 (2013) 2176–2186.
[125] S. Szczukiewicz, N. Borhani, J.R. Thome, Two-phase flow operational maps for multi-microchannel evaporators, Int. J. Heat Fluid Flow 42 (2013) 176–189.
[126] S. Kakac, B.A. Bon, A review of two-phase flow dynamic instabilities in tube boiling systems, Int. J. Heat Mass Transf. 51 (2008) 399–433.
[127] T. Zhang, T. Tong, J.Y. Chang, Y. Peles, R. Prasher, M.K. Jensen, J.T. Wen, P. Phelan, Ledinegg instability in microchannels, Int. J. Heat Mass Transf. 52 (2009) 5661–5674.